Received: 30 October 2023 | Revised: 3 March 2025 | Accepted: 5 March 2025

DOI: 10.1002/esp.70043

RESEARCH ARTICLE

ESPL WILEY

Denudation rates and Holocene sediment storage dynamics inferred from *in situ* ^{14}C concentrations in the Feshie basin, Scotland

Anya H. Towers[1] | Simon M. Mudd[1] | Mikael Attal[1] | Fiona J. Clubb[2] | Steve A. Binnie[3] | Tibor J. Dunai[3] | Negar Haghipour[4]

[1]School of GeoSciences, University of Edinburgh, Edinburgh, UK

[2]Department of Geography, Durham University, Durham, UK

[3]Institute of Geology and Mineralogy, University of Cologne, Cologne, Germany

[4]Geological Institute, ETH Zürich, Zürich, Switzerland

Correspondence
Anya H. Towers, School of GeoSciences, University of Edinburgh, Drummond Street, Edinburgh, EH8 9XP, UK.
Email: s1520260@ed.ac.uk

Funding information
Natural Environment Research Council, Grant/Award Number: NE/S007407/1; Scottish Environment Protection Agency

Summary

Scotland's Highlands are tectonically quiescent but have experienced high rates of isostatic uplift in response to deglaciation. To understand the effects of both deglaciation and regional uplift on landscape evolution, we measured the concentration of cosmogenic *in situ* ^{14}C in river sands collected in Glen Feshie (Cairngorms). Like other terrestrial cosmogenic radionuclides, *in situ* ^{14}C can be used to calculate basin-wide denudation rates over millennial timescales. ^{14}C has a short half-life relative to other *in situ* cosmogenic radionuclides, giving it an advantage in post-glacial landscapes: Very little ^{14}C will be inherited from exposure before glaciation of the landscape, meaning that concentrations will reflect sediment production and transport dominantly in the Holocene. When we calculate denudation rates based on the common assumption of basin-wide homogeneity of erosion, we find no correlation between topographic metrics such as the normalised channel steepness index and inferred denudation rates, which range between 0.175 and 1.356 mm/year. Based on field and remote sensing observations, we suggest that ^{14}C becomes diluted downstream due to sediment supply from paraglacial terrace material, and develop a mixing model to test this hypothesis. We identify the terraces that are likely to contribute sediment to the channels through flood modelling, geomorphic mapping and remote sensing observations. Our mixing model indicates that the observed distribution of ^{14}C concentrations can be explained if terrace escarpments have basin-averaged migration distances of 8 to 30 cm during large flood events. This interpretation is consistent with remotely sensed images of channel activity and terrace bank retreat within the catchment. Our results show that paraglacial sediment stores contribute to sediment fluxes in the late Holocene and highlight the on-going glacial legacy on landscape evolution.

KEYWORDS
catchment averaged erosion rates, post-glacial landscapes, sediment sources, sediment transport

1 | INTRODUCTION

Sediment delivery to river networks influences their morphology and dynamics. For example, increased sediment deposition can reduce the capacity of channels to contain floodwaters which can lead to an increase in flood hazard (Slater *et al.*, 2015; Stover & Montgomery, 2001; Raven *et al.*, 2009). In recent decades, detrital cosmogenic radionuclides (CRN) in stream sediments have been widely used to quantify catchment average denudation rates over millennial timescales (e.g., Bierman, 1994; Brown *et al*., 1995; Granger *et al*., 1996; von Blanckenburg, 2005). Rates derived from long-lived isotopes, such as ^{10}Be (half-life of ≈ 1.39 Myr, Chmeleff *et al*., 2010), reflect the weathering, erosion and fluvial transport of hillslope sediments which have been linked to climatic and/or tectonic controls in active orogenic settings (e.g., Bookhagen & Strecker, 2012; Godard *et al*., 2014; Safran *et al*., 2005; Scherler *et al*., 2014). To understand these wider controls of climate and/or tectonics on landscape evolution, studies have correlated CRN-derived erosion rates to upstream catchment characteristics, such as channel steepness, temperature and uplift rates (e.g., Cyr *et al*., 2010; Delunel *et al*., 2010; Delunel *et al*., 2020; Harel *et al*., 2016; Wittmann *et al*.2007).

Research into controls on denudation has mainly focused on non-glaciated landscapes, however, which are typically less complex than formerly glaciated landscapes. Key challenges associated with understanding geomorphic processes in low-relief, post-glacial landscapes originate from the preservation of glacially modified topography. In these landscapes, hillslopes can be decoupled from channels due to the overdeepening and widening of valleys by glaciers and extensive glacial sediment drapes (e.g., till, moraines and paraglacial terraces) influence sediment supply and transport capacity (Ballantyne, 2019; Whitbread *et al*., 2015). In many Scottish river basins, channel erosion has exposed dramatic paraglacial terraces that appear to be contributing large quantities of sediment to modern rivers (e.g., Ballantyne, 2019). Scotland has been in a phase of glacial isostatic rebound since the disappearance of the British–Irish Ice Sheet and complete deglaciation following the Loch Lomond Stadial/Younger Dryas around 12 ka ago (Ballantyne, 2019; Clark *et al*., 2018; Firth & Stewart, 2000; Shennan *et al*., 2009). Uplift rates are spatially variable across Scotland, with the highest uplift rates in the central and western Highlands (>1 mm/year average over the last 1000 years; Shennan *et al.* 2009). Base-level signals propagating inland from the North Sea do not appear to have transmitted this high uplift rate to the central Scottish ranges, however, as knickpoints presumed to be caused by the isostatic rebound are clustered around Scotland's coastlines (Bishop *et al*., 2005; Castillo *et al*., 2013). Relatively little is known about the rates and processes controlling denudation in these central ranges.

In addition to geomorphic complexity, denudation rates are also much more challenging to measure in low-relief, post-glacial landscapes such as Scotland. The use of long-lived isotopes such as ^{10}Be in these settings is problematic, because repeated phases of shielding and exposure during past glacial, interglacial and interstadial periods can lead to ^{10}Be concentrations that are difficult to interpret (Fame *et al*., 2018). For example, in the high-relief, glacial and post-glacial European Alps, where the median ^{10}Be-derived denudation rate is 0.414 mm/year (Delunel *et al*., 2020), denudation rates derived from ^{10}Be typically integrate over millennial timescales. The integration timescales are calculated by the absorption depth scale, which is generally accepted to be approximately the top 60 cm beneath Earth's surface, divided by the denudation rate (e.g., Lal, 1991). Moreover, inferred denudation rates can be corrected for cosmogenic shielding by snow and ice (e.g., Mudd *et al*., 2016) from late Holocene glacial inventories and snow cover maps. In Scotland, which has a lower relief compared to the European Alps, one would expect lower denudation rates (e.g., von Blanckenburg, 2005) meaning that ^{10}Be erosion rates would integrate over longer timescales (e.g., a denudation rate of 0.05 mm/year would integrate over 12 000 years). This means that low denudation rates derived from ^{10}Be may integrate over glacial, interglacial and interstadial cycles (e.g., Lateglacial Interstade ≈ 14.7–12.9 ka, Middle Devinsian before the expansion of the last British-Irish Ice Sheet ≈ 35 ka; Ballantyne *et al.* 2021). This leads to the potential for large amounts of uncertainty in ^{10}Be-derived denudation rates. Furthermore, the recycling of sediment as well as transport of sediment across topographic divides during multiple phases of glaciation will have occurred in post-glacial landscapes such as Scotland (Linton, 1949). As a result, sediment grains sampled at a given location may have experienced complex and different histories, making quantification of the inherited component of the ^{10}Be concentrations difficult, if not impossible.

In contrast to ^{10}Be, cosmogenic *in situ* ^{14}C has a short half-life (≈ 5700 years, International Atomic Energy Agency, 2024), which means that inferred denudation rates from ^{14}C concentrations in stream sediments will mainly reflect post-glacial, Holocene erosion. For example, approximately 90% of ^{14}C will have decayed after 20 000 years of complete burial. This technique therefore provides a new opportunity to understand landscape evolution and rates of erosion in formerly glaciated regions.

Applying ^{14}C to infer catchment-averaged erosion rates remains limited, however, because of challenges associated with constraining ^{14}C production rates and analytical methods, such as sample extraction (see Hippe, 2017, for a review). Following recent advancements in the extraction techniques and scaling of ^{14}C production rates (e.g., Lifton *et al*., 2014a; Lifton *et al*., 2023; Lupker *et al*., 2015), studies have used ^{14}C alongside ^{10}Be to identify complex erosional histories (Hippe *et al*., 2021; Kober *et al*., 2019; Slosson *et al*., 2022). An exciting application of ^{14}C is the ability to detect short-lived sediment routing and storage events (100s to 1000s of years) which would not be detectable in catchments with relatively little sediment storage and/or where erosion rates are derived from longer-lived isotopes such as ^{10}Be (Hippe, 2017; Slosson *et al*., 2022; Wittmann *et al*., 2011). For example, Slosson *et al.* (2022) suggested that lower concentrations of ^{14}C in stream sediments relative to ^{10}Be concentrations are caused by sediment shielding and storage in highly dynamic hillslope talus deposits in the Argentine Andes.

In this study, we report the first Scottish ^{14}C-derived erosion rates in the post-glacial catchment of Glen Feshie, a braided, gravel-bedded river with an abundant sequence of paraglacial terraces and local bedrock sections located in the Cairngorm mountains of Scotland. We use a nested approach with samples along the main stem and at the mouth of tributaries to assess the contributions of various geomorphic domains and the controls on erosion rates. In contrast with tectonically active landscapes with coupled channels-hillslopes where erosion rates tend to correlate with topographic metrics such as channel steepness and uplift rates to the first-order (e.g., Kirby & Whipple, 2012; Harel *et al*., 2016), we expect that a significant portion of the fluvial sediment will be sourced from paraglacial sediment stores in our study area (e.g., Ballantyne, 2002; Church & Ryder, 1972), which will affect ^{14}C concentrations. We may consider these two scenarios as end-member hypotheses: one in which rivers have incised through the glacial drape and adjusted to regional uplift rates and the other where sediment is recycled from paraglacial deposits with little modification of the underlying bedrock.

To test which of these two scenarios is more consistent with our measured detrital ^{14}C concentrations, we explore the relationships between CRN-derived sediment fluxes and basin-averaged topographic parameters, such as channel steepness. We hypothesise that if landscape denudation is driven by active bedrock incision, CRN-derived denudation rates should positively correlate with landscape steepness. We then explore the influence of paraglacial sediment supply on CRN-derived denudation rates by presenting a mixing model which mixes 'background' sediment (i.e., sediment sourced from basin-wide erosion) with terrace sediment with various ^{14}C concentrations. We assess the impact of the remobilisation of terrace sediment by first identifying the terraces that are coupled to the channel during high flows. In the model, we then vary terrace migration distances and terrace ^{14}C concentrations across a realistic range based on the constraint we have on terrace ages and historical terrace migration. We assess the sensitivity of the results to these parameters and combine these modelling results with our observations to constrain rates and processes of sediment production in Glen Feshie.

2 | STUDY AREA

The River Feshie is a tributary of the River Spey in the post-glacial western edge of the Cairngorm Mountains (Figure 1). The main channel flows ≈ 39 km mainly northwards and has a catchment area of ≈ 231 km^2. The land is managed for mostly moorland and woodland, with commercial forestry and farming in the lower reaches. The catchment typically floods throughout the year and discharges peak during the winter and spring (maximum annual discharges regularly exceed 40 m^3/s at the gauging station upstream of the confluence with the Spey). The underlying bedrock geology is composed of Moinian Schist with a small proportion of Cairngorm Granite which underlies the higher ground in the northeast (BGS, 2021). Both of these lithologies have high concentrations of quartz, making the Feshie basin an ideal setting for studying the concentrations of *in situ* ^{14}C. The Feshie is thought to have been deglaciated at the end of the Late Devensian ≈13 000 year B.P. (Young, 1975). However, it is unknown whether the catchment was glaciated during the Loch Lomond Stadial/Younger Dryas (12 900–11 700 B.P., Chandler *et al.*, 2019; Sissons, 1974). The area subsequently experienced isostatic uplift which is estimated to be >1 mm/year over the past 1000 years (Shennan *et al.*, 2009). The aftermath of the last glaciation can be observed from features such as the wide, trough-like valleys and paraglacial outwash terraces. In comparison to other UK rivers, the Feshie is exceptionally dynamic due to its abundant sediment supply and flashy flow regime (Rumsby *et al.*, 2008; Williams *et al.*, 2020).

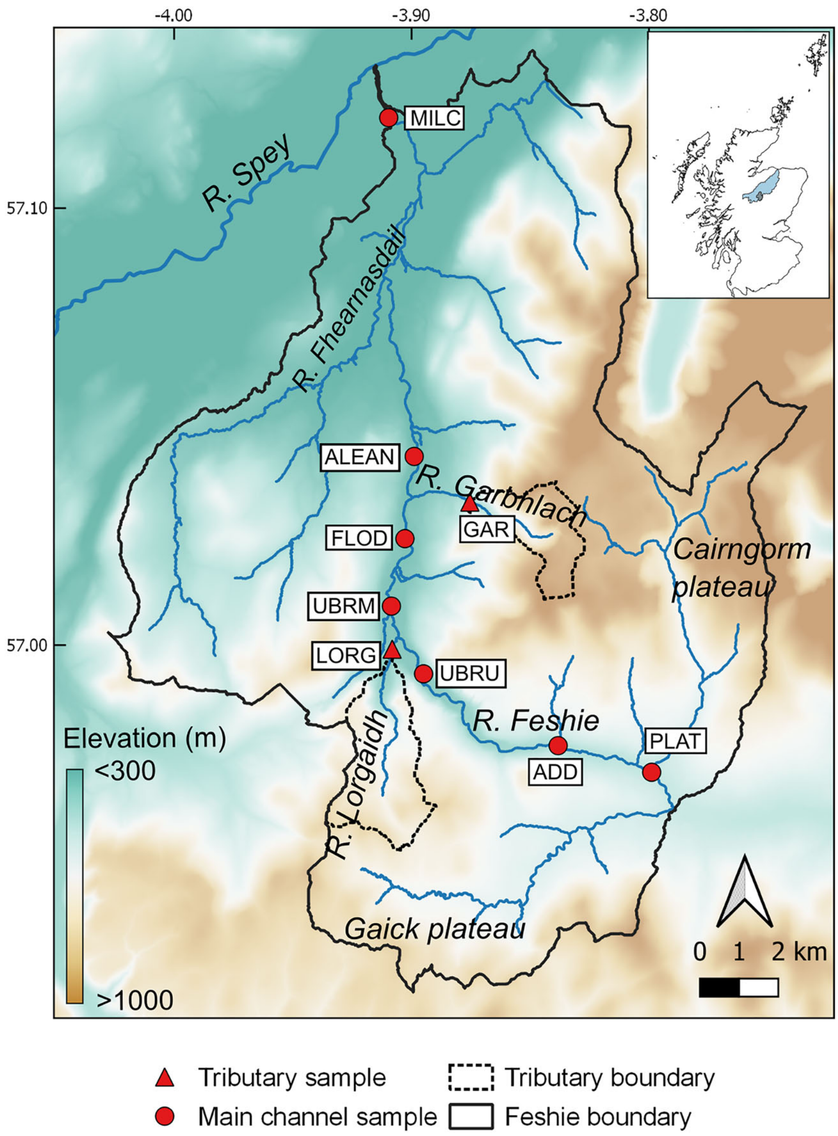

FIGURE 1 Elevation map of Glen Feshie with CRN sample locations. Red dots mark samples collected along the main river channel and red triangles represent samples collected in tributaries. Inset map shows a map of Scotland with the Spey basin coloured in blue and Feshie in grey. The 5-m Digital Terrain Model was sourced from the Ordnance Survey (Ordnance Survey, 2021).

Studies have suggested that the Feshie's paraglacial terraces represent an initial phase of net sediment deposition by meltwater streams during glacial retreat (Ballantyne, 2019; Robertson Rintoul, 1986; Young, 1976). These thick valley fills were incised throughout the Holocene leading to terrace formation. Robertson Rintoul (1986) mapped the Feshie terraces and assigned the terraces to five groups on the basis of soil-stratigraphic evidence. Robertson Rintoul (1986) suggested the older, higher terraces (Groups 1 and 2) formed at 15.6 and 11.5 cal ka BP from soil-stratigraphic comparisons and assumed deglaciation ages. Furthermore, a radiocarbon age of 4.1–3.7 cal ka BP was obtained by Robertson Rintoul (1986) for charcoal fragments within a horizon of buried soil in a lower-level terrace (Group 3) in the Lorgaidh basin (see Figure 1 for location of Lorgaidh basin) suggesting the lower-level terraces are of Late Holocene age (i.e., post-4000 years). The buried soil layer in this terrace (95 cm below terrace surface) suggests episodes of sediment aggradation then incision during the Late Holocene (Robertson Rintoul, 1986). All radiocarbon ages reported here were recalibrated using the IntCal20 calibration curve and Calib version 8.2 (Reimer *et al.*, 2020). Calibration ranges for individual radiocarbon dates represent $\pm 2\sigma$ (95.4% probability). Ages are calibrated to BP 1950.

While the modern-day dynamics of the terraces remain relatively unconstrained and there is little quantitative data on the lateral migration of the channel into these terraces, field observations and satellite imagery confirm the active nature of the channel braid plain and that terrace erosion plays a key role in providing sediment to the channels (Figure 2). For example, Figure 3 shows tens of meters of bank erosion between 2006 and 2019 for the downstream braided reach that is located upstream of the confluence with the Spey.

Measurements of terrace heights and valley fill depths suggest that the Feshie's valley is glacially overdeepened. In the upper braided reach downstream of the Lorgaidh confluence, a seismic refraction survey recorded a minimum sedimentary fill depth of 30 m below the modern-day floodplain (survey carried out by Dr. Bronwyn Matthews and Dr. Mark Naylor from the University of Edinburgh at CRN sample location FLOD using an array of wired seismic nodes and a known source consisting of a hammer and plate). Downstream of the Garbhlach confluence, a borehole survey taken from a 5-m high terrace (relative to the channel) reported a fill depth of 14.5 m before intersecting with bedrock (BGS, 2021). In contrast to the main valley alluvial fill, the Feshie basin also contains steep-sided, narrow, high-relief valleys with little sediment accommodation space such as the Garbhlach basin where the hillslopes are characterised by talus and debris flows (Figure 2). The Feshie basin also contains bedrock knickzones, such as the one labelled in Figure 2. Bedrock knickzones are a legacy of glacial erosion and are a common feature of post-glacial landscapes (Whitbread *et al.*2015).

3 | MATERIALS AND METHODS

3.1 | ^{14}C sediment sampling and processing

In this section, we describe the sampling strategy, sample preparation and ^{14}C extraction and the procedure for calculating denudation rates based on the ^{14}C concentrations.

3.1.1 | Sampling strategy

Nine quartz-rich sand samples were taken from modern gravel bars in August 2021. Samples were collected with the objective of constraining the contribution of different geomorphic domains on Holocene denudation rates in a post-glacial setting (see Section 4 for a detailed geomorphic description of the catchment). For example, sample GAR (see Figure 1 for sample names) was collected to understand the influence of a high-relief, steep landscape with relatively little valley fill on sediment fluxes. In contrast, sample PLAT was collected to isolate the influence of a low-relief setting with abundant valley fills on erosion rates. The remainder of the samples were collected downstream along the main valley-fill sequence to understand sediment source to sink fluxes.

3.1.2 | Sample preparation and ^{14}C extraction

Sample preparation and ^{14}C extraction were performed at the University of Cologne, Germany, and ETH Zürich, Switzerland. Samples were sieved and the 250–500 μm fraction was retained for *in situ* ^{14}C preparation. Samples were etched in $\approx$18 % HCl (technical grade) on a shaking table for 24 h. For the ensuing froth flotation, to remove feldspar and mica, samples were activated with 1%HF and processed with 1% AERO65 frother and Laurylamine (0.03 % v/v) using a laboratory flotation machine (MN 935/5, Humboldt Wedag). AERO65 is a completely water-soluble polyglycol type frother that produces a closely knit and persistent froth. Polyglcols are synthesised from ethylene oxide; the latter is a petrochemical product (Bailey & Koleske, 1990) that is assumed free from ^{14}C (petroleum is older than >50 kyr; thus, all ^{14}C has decayed). The resulting enriched quartz was etched twice in 5 % HF/HNO_3 on a shaking table for 24 h and twice in 1 % HF/HNO_3 in an ultrasonic bath for 24 h to obtain pure quartz (Kohl & Nishiizumi, 1992) free of organic residues from froth flotation agents (Nichols & Goehring, 2019).

We found in a previous project that fluid inclusion-rich samples can affect the integrity of the fused silica tubes used in our setup for *in situ* ^{14}C extraction, either by destructive expansion of volatiles and/or devitrification of fused silica. Devitrification of fused silica is accelerated in the presence of NaCl (Horii *et al.*, 2021). NaCl is a very common component in fluid inclusions (Bodnar & Vityk, 1984). Therefore, we now insert a temperature treatment step prior to the procedure of Fülöp *et al.* (2015), after the cleaning of samples with repeated etches in 5% HF/5% HNO_3. The etch-cleaned quartz samples are heated to 1000°C in air for 30 min, in order to decrepitate fluid inclusions (Bodnar *et al.*, 1987). This treatment also leads to the oxidation (to CO_2) of any remaining traces of organic compounds (natural or artificial) on samples' surfaces (Gulbransen *et al.*, 1963). After the heat treatment, samples are etched in 1% HF/HNO_3 overnight, rinsed with MilliQ® water and dried. The subsequent treatment and extraction follow that of Fülöp *et al.* (2015), starting with soaking the sample in concentrated HNO_3 and bringing it to dryness at 120°C.

The temperature of 1000°C and holding time of 30 min are chosen because at these conditions, the sublimation of NaCl is complete (Laptev & Bram, 2024), and any redeposited NaCl can be rinsed from

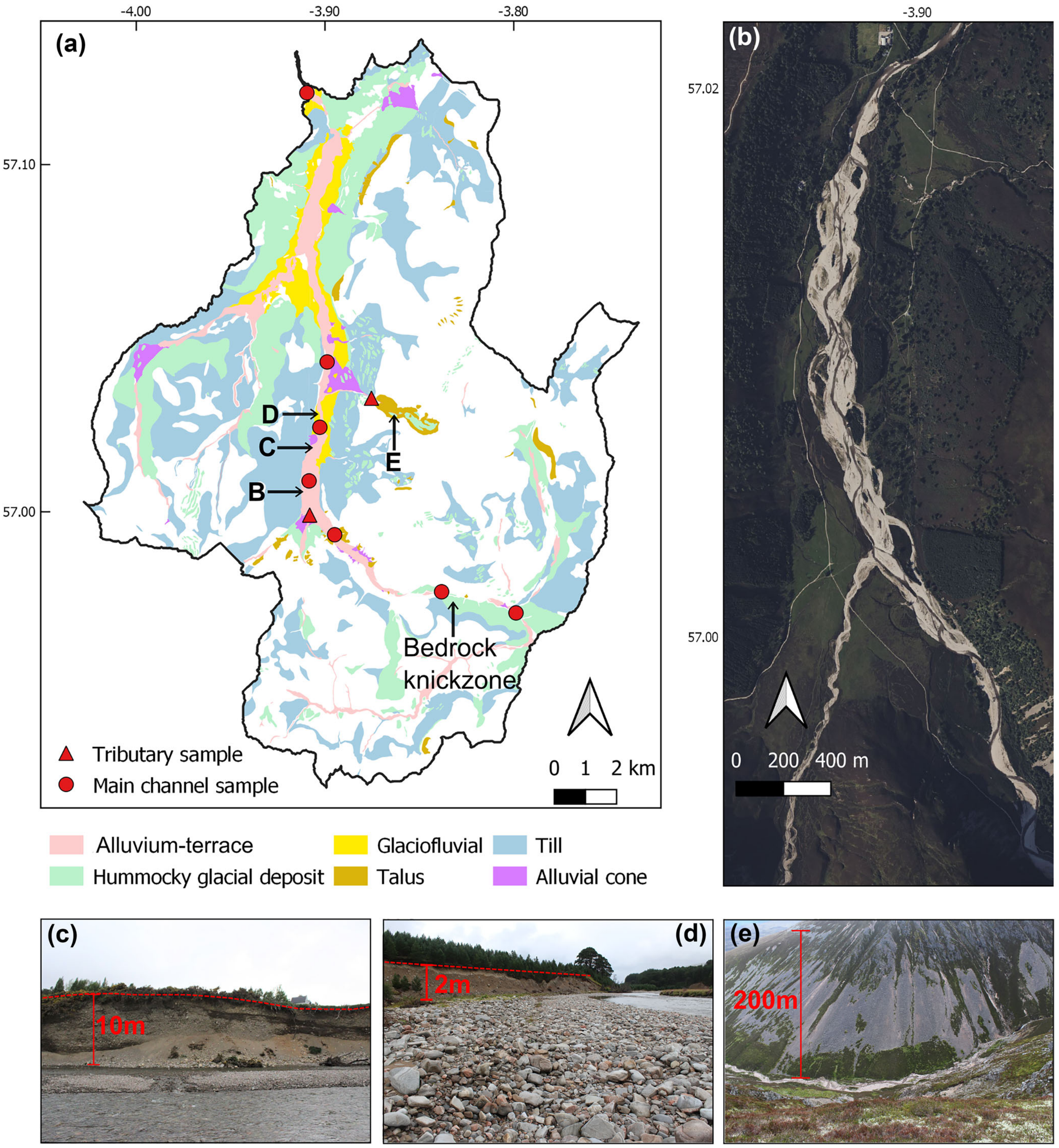

FIGURE 2 Panel (a) shows key lithological groups in Glen Feshie (lithological groups obtained from the British Geological Survey (BGS, 2021)). ≈3 km-long bedrock knickzone is marked along the main channel. "Alluvium-terrace" represents material that has been incised and reworked by channels during the Holocene, whereas "Glaciofluvial" represents material that was deposited by glacial meltwater streams and appears mostly disconnected from the modern-day channel network. Red symbols mark CRN sample locations: red dots mark samples collected along the main river channel and red triangles represent samples collected in tributaries. The locations of Figures B, C, D and E are marked on Figure A. Panel (b) shows an aerial image highlighting the characteristic braided nature of the Feshie (Bing Maps, 2023). Panels (c) and (d) show terraces which are actively feeding material into the channel. Both terraces appear paraglacial and are poorly bedded and unsorted (i.e., contain a wide range of grain sizes and angular to sub-rounded clasts with no preferential orientation direction in places). The surface of the terraces in (c) and (d) is marked by a red dashed line and their approximate heights are also shown. Panel (e) is a photograph of the steep, high-relief Garbhlach basin where the hillslopes are characterised by bedrock and talus deposits.

the sample with aqueous solutions. We tested this approach utilising aliquots of two surface quartz samples (vein quartz, Atacama Desert, crushed to identical grain-size as utilised in the current study), heating one aliquot of each to 1000°C (30 min) and not heating the others. We found no discernible differences between the extracted amounts of ^{14}C, with the samples identified as RL13-001 & RL17-024 yielding the following concentrations: 170 ± 4 versus 165 ± 5 and 161 ± 4 versus $164 \pm 5 \times 10^3$ atoms ^{14}C/ g quartz ($\pm 1\delta$), where the first number

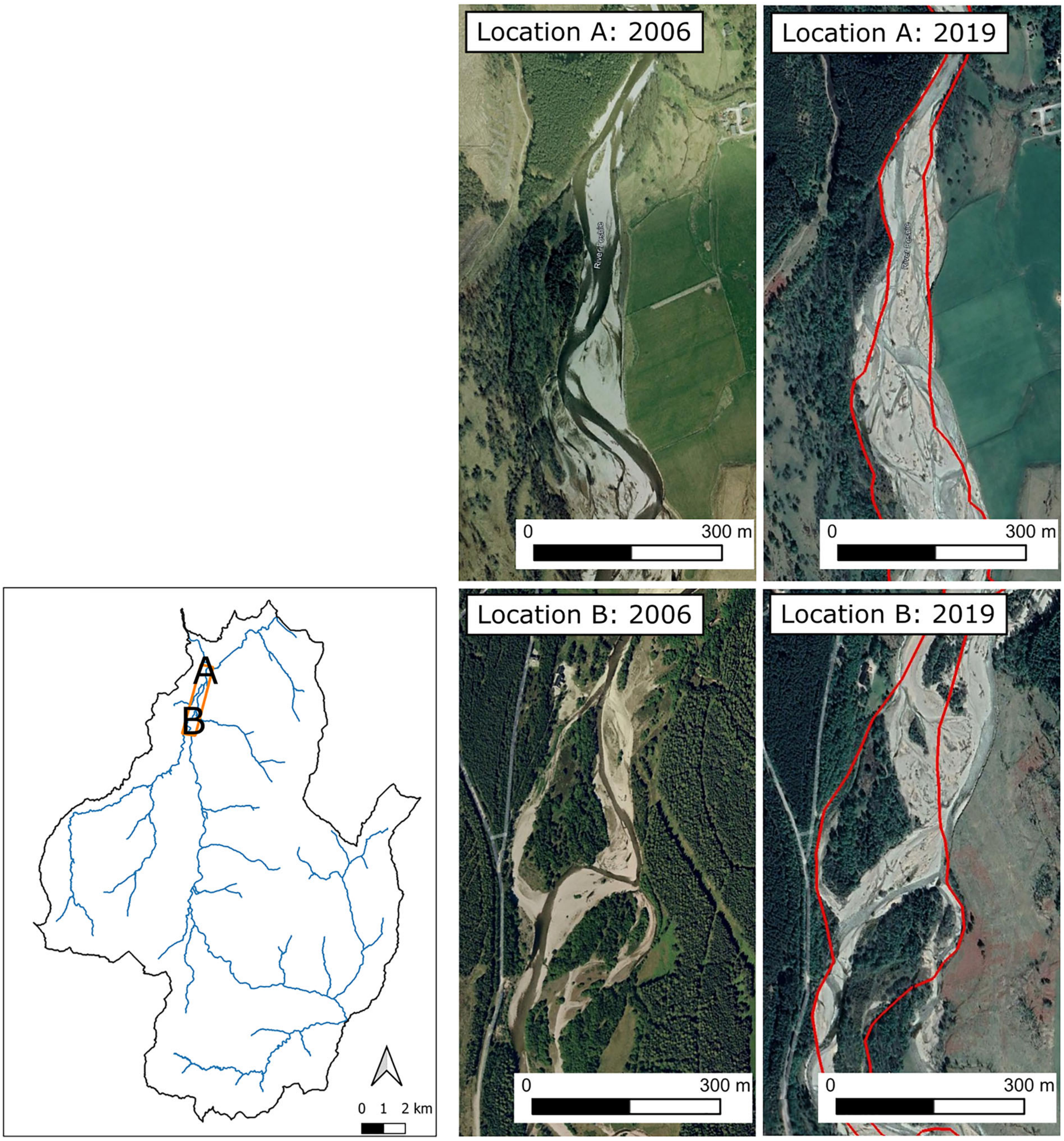

FIGURE 3 Evidence of meter-scale channel change from Google Earth Imagery (Google Maps, 2023) between 2006 and 2019 in the downstream braided reach (orange box on inset map). Red line on 2019 imagery marks the approximate extent of the 2006 bankfull channel. Tens of meters of bank migration is observed, especially at location B, which could have been enhanced by the felling of plantation woodland. Imagery dates were selected following the limited availability of clear, cloud free images.

in each pair is the result of samples pre-treated at 1000°C and the second number the result without pre-treatment. Hence, we find no indication that *in situ* ^{14}C is lost by volume diffusion from quartz during the pretreatment (1000°C, 30 min, in air).

We are aware of conflicting claims that *in situ* ^{14}C is lost from quartz at low temperatures, above 500°C (Lifton *et al.*, 2001; Lifton *et al.*, 2023), but that there is no loss of *in situ* ^{14}C below 900°C (Hippe *et al.*, 2013). The data of Lifton *et al.* (2001) (Figure 6 therein), on which the claim of loss above 500°C is mainly based (Lifton *et al.*, 2001; Lifton *et al.*, 2023), show an essentially flat release pattern of ^{14}C between 500°C and 1200°C for two splits of a surface sample, that is, the observed release of ^{14}C does not increase with temperature in this wide temperature range. Volume diffusion in solids, however, accelerates (exponentially) with increasing temperature (Mehrer, 2007). Therefore, volume diffusion, that is, loss of *in situ* ^{14}C from the lattice, cannot be the process responsible for the observed low-temperature release of ^{14}C in (Lifton *et al.*, 2001). A possible source for the ^{14}C released at low temperatures (Lifton *et al.*, 2001; Lifton *et al.*, 2023) could be organic compounds from endolithic biota carrying ^{14}C (Mergelov *et al.*, 2018). Endolithic algae/fungi/bacteria are pervasive in surface rocks, even in the most extreme environments (Wierzchos *et al.*, 2013). Nichols and Goehring (2019) have demonstrated that the commonly applied treatment with 1% HF/1% HNO3 in quartz purification protocols (Kohl & Nishiizumi, 1992) is insufficient for reliably removing organic compounds to the level required of *in situ* ^{14}C analysis (laurylamine in the study of Nichols &

Goehring; 2019; laurylamine has no specific affinity to the surface of quartz Sulaymonova *et al.*, 2018). The samples in Lifton *et al.* (2001) and Lifton *et al.* (2023) that show a low-temperature release of ^{14}C were treated with 1% HF/1% HNO3 (PP4 in Lifton *et al.*, 2001; CRONUS-A in ; Lifton *et al.*, 2023; preparation of CRONUS-A described in ; Jull *et al.*, 2015); one material (CoQtz-N), which was more aggressively leached (2% HF/2% HNO_3 to 15% weight loss, starting with pure quartz Binnie *et al.*, 2019), did not show a ^{14}C release at low temperature (Lifton *et al.*, 2023). The importance of clean intercomparison materials has been pointed out recently (CRONUS-N; Corbett *et al.*, 2022). It is beyond the scope of this study to resolve this issue conclusively. Relevant for the current study is that we are unaware of any data published showing a low-temperature ($\leq$ 1000°C) release (pattern) of ^{14}C from quartz that would conform with the physics of diffusive transport in solids.

The pure quartz samples ($\approx$4 g each) were extracted subsequently for gas-source accelerator mass spectrometer (AMS) analysis in a custom build extraction line at the University of Cologne following the procedure described in Fülöp *et al.* (2015). As per Fülöp *et al.* (2015), carbonate was added before processing. Blanks were analysed at the Cologne AMS facility (Schiffer *et al.*, 2020) and samples for this study at the ETH Zürich (Lupker *et al.*, 2019; Wacker *et al.*, 2013). As is common practice since the onset of AMS technology in the 1980s, both AMS facilities are calibrated with standard materials. Both laboratories participate in international laboratory intercomparisons (Scott *et al.*, 2018). Both facilities use NBS-Ox II standard material for calibration. The background measurement from full processed blanks, which was obtained by the repeated extraction of synthetic quartz (Schiffer *et al.*, 2020), is 38 000 ± 10 000 atoms ^{14}C ($\pm 1\delta$, $n = 26$; measurements since 2020).

We refer the reader to Supporting Information Table S3 for information on the blank measurements.

3.1.3 | Denudation rate calculations

Catchment-averaged denudation rates were calculated from each sample's ^{14}C concentration using the CAIRN (Catchment-averaged denudation Rates from cosmogenic Nuclides) method (Mudd *et al.*, 2016). CAIRN calculates analytical solutions of a statement of conservation of nuclide concentration through time *t*:

$$\frac{dC_j}{dt} = P_j - \lambda_j C_j \tag{1}$$

where C_j is the concentration of nuclide *j* (in this case ^{14}C) in units atoms per gram, P_j is the nuclide production rate in units atoms per gram per year and λ_j is the nuclide decay coefficient (in units 1/year). This approach is similar to that of Parker (1991), but after applying simplifying assumptions, solutions to this equation reduce to more widely used derivations such as Lal (1991) and Granger and Smith (2000).

Nuclide production is a function of latitude, altitude (or atmospheric pressure), geomagnetic field strength and shielding by rock, soil, vegetation, water and/or snow (e.g., Balco *et al.*, 2008). Nuclide production can be caused by both neutrons and muons (e.g., Gosse & Phillips, 2001). CAIRN calculates production following the relatively simple approach of an approximation using four summed exponential functions, similar to a number of authors (Braucher *et al.*, 2009; Granger & Smith, 2000; Schaller *et al.*, 2009; Vermeesch, 2007):

$$P_j(d) = P_{j,SLHL} \sum_{i=0}^{3} S_{i,j} F_{i,j} e^{\frac{-d}{\Lambda_i}} \tag{2}$$

where $P_{j,SLHL}$ is the total surface production rate (atoms g^{-1} year^{-1}) at sea level and high latitude, $F_{i,j}$ is a dimensionless scaling that relates the relative production of neutron spallation and muon production, $S_{i,j}$ is a dimensionless scaling factor that combines the effects of production scaling and shielding of cosmic rays, *d* is a mass per unit area which represents the mass overlying a point under the surface (typically reported in g cm^{-2}) and Λ_i is the attenuation length for reaction type *i* (g cm^{-2}). The reaction types are $i = 0$ for neutrons and $i = 1-3$ for muons.

The depth *d*, called shielding depth, is related to depth below the surface as follows:

$$d = \int_{\zeta-\eta}^{\zeta} \rho(z)\,dz \tag{3}$$

where ζ (cm) is the elevation of the surface, η (cm) is the depth in the subsurface of the sample, *z* (cm) is the elevation in a fixed reference frame and ρ (g cm^{-3}) is the material density, which may be a function of depth. The shielding depth is typically reported in g cm^{-2}. For a constant density, $d = \rho\eta$.

Combining Equations (1) and (2) results in a partial differential equation that can be solved analytically.

One simple scenario is when the denudation rate, ϵ, (g cm^{-2} year^{-1}) is constant in time. The general solution for this scenario for the concentration of a nuclide at depth *d* and time *t* that had a starting position at depth d_0 and an initial concentration C_0 at time t_0 is as follows:

$$C(t) = C_0 e^{-(t-t_0)\lambda_i} + P_0 \left[\sum_{i=0}^{3} \frac{S_i F_i \Lambda_i}{\epsilon + \Lambda_i \lambda} e^{\frac{-d_0}{\Lambda_i}} \left(e^{\frac{\epsilon(t-t_0)}{\Lambda_i}} - e^{-(t-t_0)\lambda} \right) \right] \tag{4}$$

We have dropped the subscript *j* indicating the nuclide for simplicity; subsequent equations apply to any nuclide. Equation (4) is the same as Equation (11) in Mudd *et al.* (2016). We can use Equation (4) to derive more complex erosion scenarios that might occur in a transient landscape.

For computing the apparent erosion rate, CAIRN further assumes constant erosion rates beginning at infinite depth and infinite time ($t_0 = 0$ and $t = \infty, d_0 = \infty$), reducing the equation to the following:

$$C(d) = P_{SLHL} \sum_{i=0}^{3} \frac{S_i F_i \Lambda_i e^{-d/\Lambda_i}}{\epsilon + \lambda \Lambda_i} \tag{5}$$

where ϵ is the denudation rate (g cm^{-2} year^{-1}). If we set $d = 0$ (i.e, we solve for material being eroded from the surface, with no distributed mass loss via chemical weathering), Equation (5) reduces to equation (6) from Granger and Smith (2000) for denudation only (i.e., no burial or exposure) and reduces to Equation (8) of Lal (1991) if production is due exclusively to neutrons.

CAIRN does include modules for topographic shielding, but DiBiase (2018) demonstrated that the shorter attenuation length from steep slopes cancels topographic shielding so we do not reduce production from topographic shielding to calculate denudation rates. CAIRN then calculates the production rate for each pixel based on an effective attenuation depth following the approach of Vermeesch (2007). We calculate the surface production scaling, S_{tot}, using the scaling of Lal (1991) and Stone (2000). It should be noted that the Lal/Stone (LSt) scaling is time invariant. Nuclide production is, however, known to vary with the intensity of Earth's geomagnetic field, which is taken into account in other scaling schemes such as the Lifton/Sato/Dunai (LSD) which take into account time-varying production rates (Lifton *et al.*, 2014b). The recent studies of Charreau *et al.* (2019) and Stbner *et al.* (2023) have shown that failing to account for time-varying production can lead to large changes in inferred erosion rates using ^{10}Be. However, the difference between the LSt scaling and LSD scaling is relatively low at high latitude sites such as ours (<10%) and where erosion rates vary by less than an order of magnitude (Charreau *et al.*2019; Stbner *et al.*, 2023). Neither of these two studies explored the effect on ^{14}C, but this assumption is consistent with other research showing geomagnetic fluctuations for nuclides make little difference at latitudes higher than 50 degrees (Dunai, 2010).

The scaling terms for individual production mechanisms, S_i, may vary depending on elevation, shielding, sample thickness or denudation rates. For example, muogenic pathways will contribute relatively more to production when there is more shielding since muogenic reactions penetrate deeper than spallation. Following Vermeesch (2007), we calculate a single surface production rate, S_{tot}, that combines production scaling and topographic shielding and then partition this total production to individual scaling terms by employing a virtual attenuation length, Λ_v, in units of g cm^{-2}:

$$S_i = e^{\frac{-\Lambda_v}{\Lambda_i}} \tag{6}$$

We then calculate Λ_v based on S_{tot}. S_{tot} is calculated using the Lal/Stone scaling, but this is calculated using the spallation production rate reported by Borchers *et al.* (2016) and dividing this by the fraction of production from spallation from Lupker *et al.* (2015), that is, 12.24 atoms/g/year divided by $F_0 = 0.788$ to arrive at a P_{SLHL} of 15.533 atoms/g/year. We then calculate the individual production mechanisms such that

$$S_{tot} = \sum_{i=0}^{3} S_i F_i \tag{7}$$

In Equation (7), S_{tot} and F_i are known, whereas S_i are functions of Λ_v. We thus iterate upon Λ_v, calculating S_i using Equation (6) using Newton's method until Equation (7) converges on a solution for Λ_v.

We can then calculate the production of atoms of ^{14}C at every pixel in our DTM using Equation (5). We make an initial guess at the denudation rate, ϵ, based on simple denudation rate estimates from Lal (1991), and then we use the Newton–Raphson iteration to converge on the observed concentrations in a given basin by changing the ϵ value. The full method is described in Mudd *et al.* (2016). The parameter values used for the scaling and production are shown in Table 1. Note that for *in situ* ^{14}C, the F_2 and F_3 parameters are zero; Lupker *et al.* (2015) found that the production curve could be represented with only one muon production pathway (negative muon capture).

We report uncertainties on the denudation rates by calculating denudation rates from the reported ^{14}C concentrations $\pm$ the blank-corrected uncertainty values. We refer the reader to Supporting Information Table S1 for a glossary of all the symbols outlined in this section.

3.2 | Basin-averaged topographic parameters

As described in Section 4, studies in mountainous landscapes have found that denudation rates tend to correlate with topographic metrics such as channel steepness and elevation (e.g., Cyr *et al.*, 2010; Delunel *et al.*, 2010; Delunel *et al.*, 2020; Harel *et al.*, 2016; Wittmann *et al.*, 2007). For example, Delunel *et al.* (2010) found a correlation between denudation rates and mean basin elevation in the Western French Alps, from which they suggested frost-shattering to be the main driver of denudation rates in their study area. For each sample, we determine the upstream contributing basin area and then calculate basin-averaged topographic metrics from the 5-m Digital Terrain Model (DTM) from the Ordnance Survey (Ordnance Survey, 2021). Basin area, elevation (proxy for temperature), slope and channel steepness were derived from the DTM in LSDTopoTools (Mudd *et al.*, 2023). We calculate the normalised channel steepness index, k_{sn}, which is the channel slope normalised to drainage area and typically reflects the erosive ability of a channel (Flint, 1974; Wobus *et al.*, 2006). We use the algorithms from Mudd *et al.* (2014) to calculate k_{sn}, using a concavity index of 0.45 (Mudd *et al.*, 2014). A map of channel steepness across the Feshie basin is available in Figure S1 in the Supporting Information.

3.3 | Terrace mixing model

Erosion rates derived from ^{14}C concentrations in catchments with little valley fill (e.g., Garbhlach tributary) can be reasonably assumed to represent catchment-wide denudation rates. However, as described in Section 4, the Feshie contains an abundant sequence of paraglacial terraces along the main channel and along the Lorgaidh and Fhearnasdail tributaries. To test whether these terraces are contributing significant quantities of sediment to the modern channel and affecting the detrital ^{14}C concentrations, we present a mixing model which mixes the 'background' sediment with terrace sediment. The 'background' erosion rate reflects sediment sourced 'basin-wide' from erosion of channels and hillslopes with no contribution from transient sediment stores. In this section, we first present the model, followed by the methodologies to obtain terrace bank heights, lengths and ages which will all influence the output of the mixing model.

3.3.1 | Description of model and assumptions

We hypothesise that samples along the main channel and River Lorgaidh will provide faster apparent catchment-averaged erosion rates than they should because they will contain sediment with background ^{14}C concentrations mixed with lower concentration material from terraces bordering the channels. We hypothesise that the terrace material has lower CRN concentrations because (1) the production of CRN in terrace materials decreases with depth (see cartoon diagram in Figure 4) and (2) terrace materials have remained buried until the last phase of major incisio and were therefore largely shielded from cosmic rays (i.e., 'fill-cut' terraces; see Section 4 for further discussion).

To test our overarching hypothesis of low ^{14}C concentration terrace material mixing with high ^{14}C concentration 'background' material, we perform a mass balance calculation for each sample (except GAR which is from a catchment that is largely devoid of terrace material) which calculates a drainage basin's ^{14}C outlet concentration, C_{Basin}, by mixing the 'background' sediments with terrace sediments. Our approach is similar to the theoretical model outlined by Wittmann and von Blanckenburg (2009), who proposed a method to detect sediment storage and transfer in depositional basins from ^{14}C. Our model assumes that both terrace sediments and 'background' sediments have similar concentrations of quartz and that there have been no differences in the chemical depletion rates among sediment sources.

Assuming all sediments are well-mixed, the concentration of ^{14}C in the collected sediments, C_{basin}, is equal to the number of atoms supplied to the sampling site divided by the mass of sediment supplied. We assume that the sample is composed of atoms (α) and masses (M) of ^{14}C supplied by background erosion (α_{bg}, M_{bg}) and terrace erosion (α_f, M_f). The timing and frequency of terrace erosion is largely unknown in the catchment. For example, terraces could erode progressively through time (i.e., low magnitude, high frequency scenario) or only erode during major flood events (high magnitude, low-frequency scenario). Field observations suggest that both scenarios are likely: We observe sloped sediment deposits at the base of terraces, indicating a more progressive system and also observe undercut terraces, suggesting flood events drive geomorphic change. For the purpose of this study and the mixing model proposed, we assume that terrace sediment was sourced from the last major flood event before sample collection, the details of which are outlined in Section 4. Also supporting this assumption is the fact that, when observed, the accumulations of debris at the toe of terrace scarps (which testify to progressive terrace erosion) tend to be disconnected from the active channel, that is, not in contact with the flowing water at low flow. This sediment may therefore become incorporated only during major floods, even if it has progressively accumulated between two major floods.

C_{basin}, in atoms per gram, is given by the following:

$$C_{Basin} = \frac{\alpha_{bg} + \alpha_f}{M_{bg} + M_f} \tag{8}$$

The mass supplied in the last flood event from the terraces is the sediment density times the volume transferred to the channel. For convenience, we use units of g/m^3 for density, which allows us to match unit conventions for measuring CRN concentrations and distances. The units of density in these equations cancel as they appear in both top and bottom terms of the fraction in Equation (8), so they are, in practice, arbitrary. The volume from the terraces is the product of the migration distance (D_T in meters), the height of the terrace bank relative to the channel (H_T in meters) and the length of the eroded terrace (L_T in meters). The model assumes that the terrace walls are vertical (see Figure 4). The number of atoms supplied is this mass times the concentration of ^{14}C in the terrace (C_T, in atoms/gram). The mass of the sediment supplied from the 'background' at the sampling point is the erosion rate (E_{bg}, units m/year) times the time since the last flood, ΔT, times the upstream area (A in m^2), times the sediment density (g/m^3). The number of atoms supplied from the 'background' at

TABLE 1 Parameters used in CRN calculations.

Parameter	Value
$P_{0,SLHL}$	15.533 atoms/g/year
F_0	0.788
F_1	0.212

Note: The length scales for spallation and muogenic production are 160 and 1500 g/cm^{2}for F_0, F_1, respectively. The relative scaling parameters are from Lupker et al. (2015). Note that in this scheme F_2 and F_3 are zero. The total production rate at high latitude and sea level is calculated using the production from the Lal/Stone scaling reported for spallation in Borchers et al. (2016) divided by the spallation scaling, F_0. The decay coefficient is 1.2158^{-4} year^{-1}.

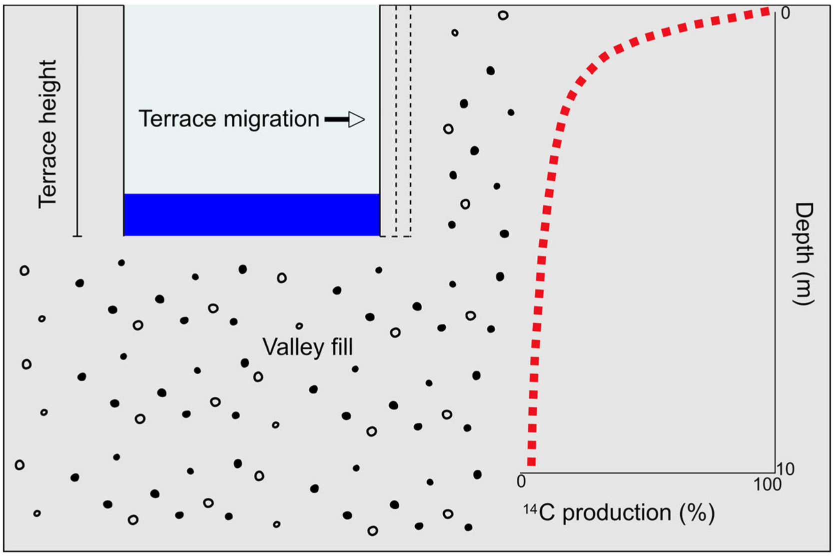

FIGURE 4 2D cartoon diagram showing the terrace components of our model, modified from Wittmann and von Blanckenburg (2009). The production of ^{14}C is shown to decrease with depth (red dashed line, production curve taken from Hippe, 2017). Terrace height H_T, terrace migration distance in the time period considered D_T, and terrace length L_T (not shown because our cartoon is 2D) control the concentration of the terrace material entering the river in our model. Valley fill depth is not to scale because it is largely unknown and likely to be spatially variable.

the sampling point are this mass times the concentration in the background (C_{bg}). Note that all these terms include the density, which we assume to be the same for both the 'background' and terrace sediment, so these terms cancel, resulting in the following:

$$C_{Basin} = \frac{C_{bg}E_{bg}A\Delta T + C_T L_T H_T D_T}{E_{bg}A\Delta T + L_T H_T D_T} \quad (9)$$

In Equation (9), the numerator is in units atoms m^3/g and the denominator is in units m^3, so the units of C_{basin} are atoms/g. To calculate the background concentration, C_{bg}, we need to assume a given background erosion rate; we then use CAIRN to solve for the concentration at the sampling point. We note in this stage that the sample GAR could be a good candidate for this assumed background erosion rate, as its upstream area is relatively devoid of terraces (Figures 1 and 2) and ^{14}C concentrations will likely represent catchment-wide denudation rates, as will be discussed. The methods for obtaining terrace bank heights, lengths and concentrations are outlined in Section 4. Terrace migration distances are largely an unknown, so we model a range of migration distances and discuss these in relation to terrace concentrations in Section 4. Variations in terrace bank migration distances, ages and heights are expected to cause differences in ^{14}C concentrations (and apparent denudation rates) between sites that have recorded a paraglacial terrace signal.

3.3.2 | Methods for obtaining terrace bank heights and lengths

As highlighted above, we assume that sediment was sourced and transported from the terraces during the last major flood event before sample collection. To obtain the lengths (L_T) and heights (H_T) of the terrace banks connected to the channel network during this flood event, we create a flood extent map. The following section describes the flood modelling and terrace extraction methodology.

To document flood trends prior to sample collection, we download discharge and rainfall data from UKCEH (https://nrfa.ceh.ac.uk/data/station/peakflow/8013) for the gauging station at Feshiebridge (located near MILC sample in Figure 1, also marked on Figure 9). The discharge time-series (Figure 5) shows that the last major flood event (February 2021, 86.99 m^3/s) had occurred 6 months before sample collection in August 2021. This flood event is equivalent to a ≈ 1 in 5-year flood event (see Figure S2 in the Supporting Information). We simulate the flood extent associated with this discharge in HAIL-CAESAR on the 5-m DTM. HAIL-CAESAR is a hydrodynamic landscape evolution model which is derived from the CAESAR-Lisflood model (Coulthard *et al.*, 2013).

We run the model in 'catchment mode' which requires the input of rainfall to generate runoff. Rainfall data were unavailable for the February 2021 flood event so we use rainfall data from a flood event in September 2009 when a similar discharge of 86.6 m^3/s was recorded. We run the model with rainfall 20 days prior to the flood event with a Manning's roughness value of 0.04 which represents mountain rivers with gravels, cobbles and boulders (Chow, 1959). We set the topmodel *m* value, which controls the peak and duration of flood events, to 0.001 which represents high infiltration rates for high, flashy flood peaks (Beven, 1997). With these parameters, including a high topmodel *m* value, the simulated peak discharge was 62 m^3/s, which highlights the potential of spatially heterogeneous rainfall. Because we are interested in mapping the flood extent associated with a 86.6 m^3/s flood, rather than replicating the precise flow dynamics, we increased the rainfall by 30%, which produced a simulated discharge of 82 m^3/s which is very close to our target discharge. We refer the reader to the Supporting Information for the simulated flood hydrograph (Figure S3).

To obtain the height of the terrace banks relative to the channel, we create a 10-m buffer around the modelled flood extent and sample this 10-m buffer every 5 m to create nodes. We then clip the nodes to the BGS alluvium/terrace dataset (BGS, 2021). We choose a buffer distance of 10 m to account for sloped sediment deposits between the terraces and the edge of the simulated flood extent, based on satellite and field observations (Figure 6). Many of the exposed terrace faces along the river are near vertical (see Figure 2), but we use a 10-m buffer to ensure that we capture the top of the terrace surfaces reliably. For example, even for a 45° terrace scarp, we would still capture a 10-m-high terrace. We then compare the elevation of each 5-m

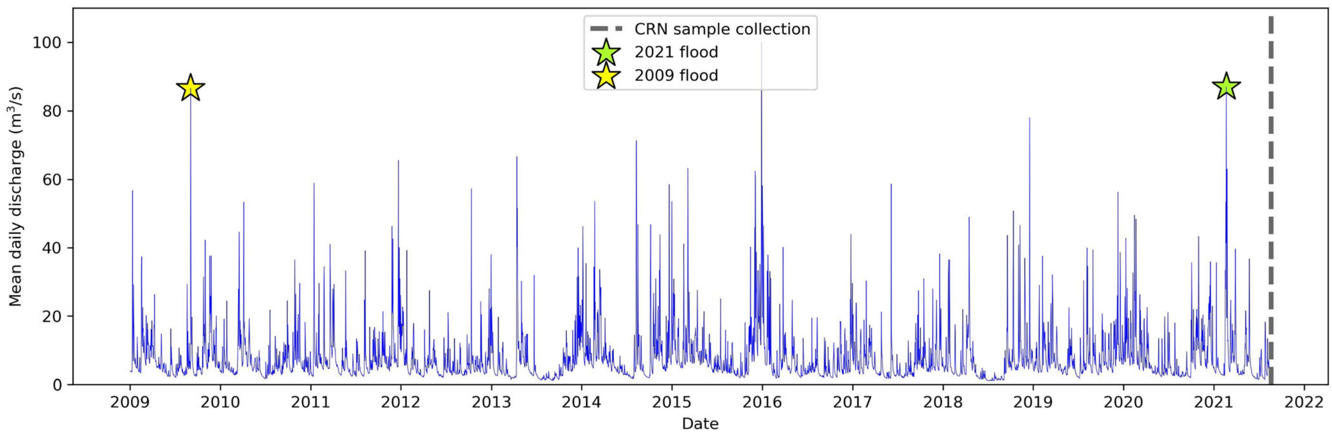

FIGURE 5 Mean daily discharge recorded at the Feshiebridge gauging station (near MILC sampling point, also marked on Figure 9). Discharge data (and rainfall) were sourced from the UKCEH (https://nrfa.ceh.ac.uk/data/station/peakflow/8013). The green star shows the most recent major flood event prior to sample collection which is a ≈ 1 in 5-year flood event. The flood modelling in this study is based on the 2009 event (yellow star) because no rainfall was available for the 2021 event (see Figure S4 in the Supporting Information for available rainfall data).

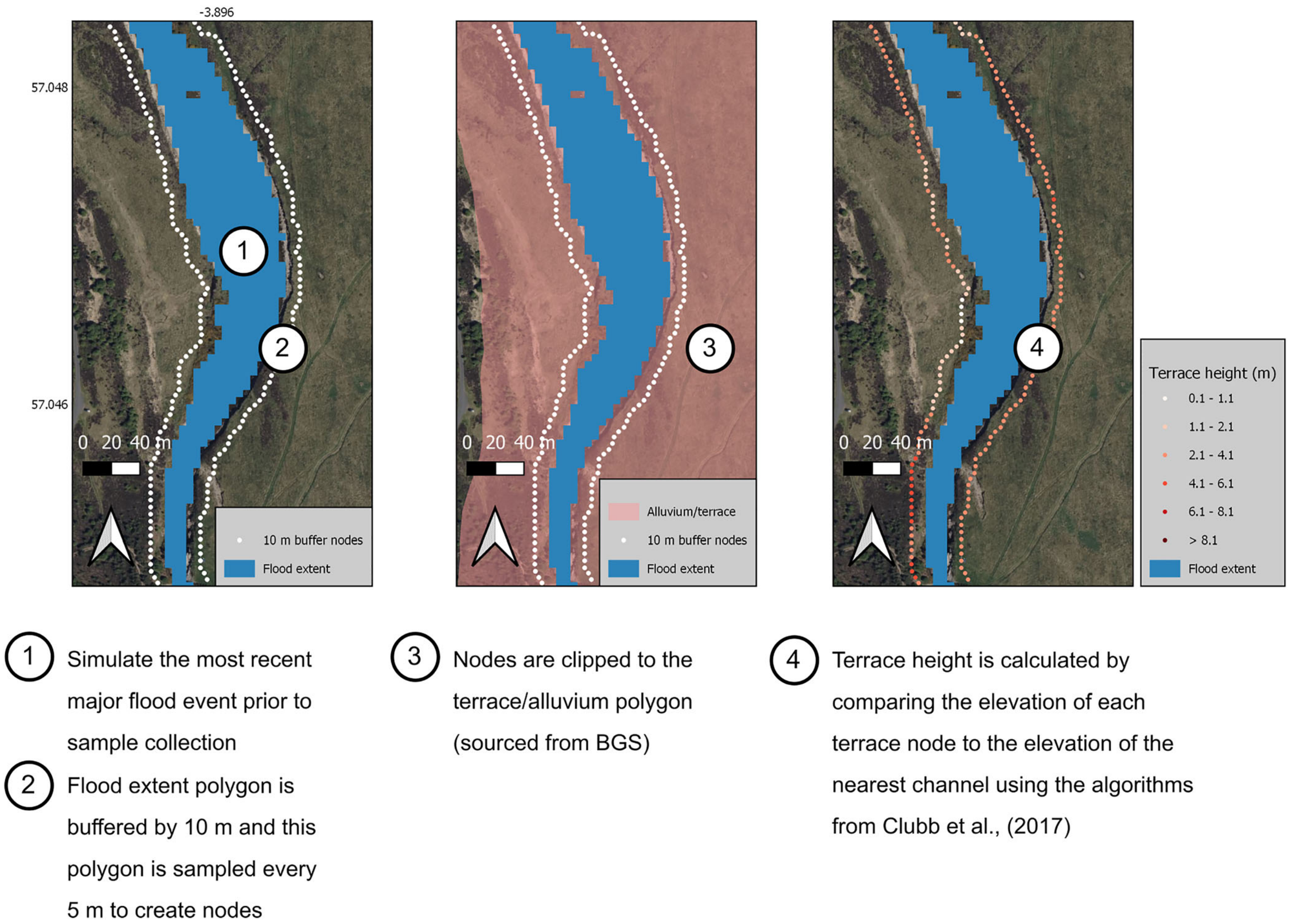

FIGURE 6 Flood modelling methodology used to infer the approximate height of terrace banks bordering the channel in the Feshie basin. We simulate a 1 in 5-year flood event (shown by the blue 'Flood extent' polygon) in HAIL-CAESAR which represents the approximate return period of the last major flood event prior to sample collection. This flood extent is then buffered by 10 m and the resulting polygon is sampled every 5 m to create nodes ('10-m buffer nodes'). These nodes are then clipped to the terrace/alluvium polygon which was sourced from the BGS (see Figure 2 for the alluvium/terrace extent of the Feshie catchment, BGS, 2021). To obtain the height of the terrace banks, the elevation of the terrace nodes is compared to the elevation of the nearest channel using the algorithms from Clubb *et al.* (2017).

terrace bank node to the nearest channel's elevation (which was derived from the DEM) using the steepest descent flow routing algorithm presented by Clubb *et al.* (2017). We will refer to this height as terrace height in the rest of the paper.

3.3.3 | Methods for obtaining terrace concentrations

The mixing model presented in Equation (9) requires terrace concentrations, C_T, to model a basin's outlet concentration, C_{basin}. The concentration of ^{14}C in terraces is mostly a function of the exposure time to cosmic rays. We explore an end-member scenario, whereby the sediment in the terraces has been shielded before exposure as the fill-cut terraces were formed. In this experiment, we assess whether incorporation of terrace material with the lowest ^{14}C concentration possible could explain the observations. ^{14}C inheritance in the terraces may be spatially variable and there is no data regarding these concentrations, hence the choice of this conservative scenario.

The timing of late Holocene major incision events and thus lower-level terrace (exposure) ages are largely unknown. To our knowledge, only one terrace date in the Feshie basin has been published: A radiocarbon age of 4.1–3.7 cal ka BP was obtained by Robertson Rintoul (1986) for a lower-level terrace (Group 3) in the Lorgaidh basin, suggesting that the lower-level terraces are of Late Holocene age (post-4000 years). Robertson Rintoul (1986) also inferred a younger terrace group of 900 cal ka BP to exist from soil stratigraphic mapping (Group 4). Both of these terrace groups (1000 and 4000 years) were interpreted to border the modern-day channel in the mapped extent which focused on the upper braided reach and Lorgaidh basin (location B in Figure 2). These results imply that the channel receives sediment from terraces aged at both 1000 and 4000 years. Based on these findings, we tentatively model our terrace bank migration distances with terrace ages of 1000 and 4000 years and discuss the implications in Section 4.

We simulate the concentration of ^{14}C in terraces using a column model available in LSDTopoTools (Mudd *et al.*, 2023). This model follows the same governing equation as Equation (4), but in this case, we simulate ^{14}C concentrations as a function of depth over a fixed duration ($t - t_0 = t_t$, where t_t is the age of the terrace) such that the governing equation reduces to the following:

$$C(t_t,d) = C_0 e^{-t_t\lambda_i} + P_0\left[\sum_{j=0}^{3} \frac{S_i F_i \Lambda_i}{\epsilon + \Lambda_i \lambda} e^{\frac{-d}{\Lambda_i}} \left(e^{\frac{\epsilon t_t}{\Lambda_i}} - e^{-t_t\lambda}\right)\right] \tag{10}$$

We therefore assume minimal denudation over the age of the terrace ($e \sim 0$) in the column model. The scaling and production parameters for this component of the study are shown in Table 1. The column model is evolved from the particle-based model presented in Mudd (2017) but includes the more rigorous production and scaling mechanisms from Mudd *et al.* (2016).

The mixing model presented in Equation (9) assumes that the total height of a terrace column, D_T, collapses into the river during a flood event. We therefore sample the column's ^{14}C concentration every 0.05 m, following which we calculate a depth-averaged concentration (C_T in Equation (9)). The column model assumes that there is no mixing or bioturbation within the terrace deposits. This assumption is supported by the fact that, when observed, terraces in the Feshie appear paraglacial and are largely composed of unsorted gravels, with very little soil relative to the total terrace height (Figure 2). Moreover, if mixing is present within a thin soil layer, then the depth-averaged ^{14}C concentration of a terrace is likely to resemble that of an unmixed terrace profile (Hippe, 2017).

We set the elevation and height of the column to the average elevation and height of the terraces in the Feshie as defined in the terrace bank extraction method section (Section 4). We also perform a sensitivity analysis to test the influence of terrace elevations (i.e., production rates of ^{14}C) on the terrace concentrations.

As discussed, we assume that there is no initial ^{14}C concentration, on the basis that the material was buried deep enough before the formation of the terrace such that all pre-existing ^{14}C had decayed. This latter assumption may not perfectly reflect reality: Terraces will have accumulated a small percentage of ^{14}C during their burial phases from deep production by muons (see Figure 4). For example, the total *in situ* ^{14}C concentration at 10-m depth is <5% of the surface nuclide production (Figure 4, Hippe, 2017). Moreover, Robertson Rintoul (1986) documented a buried soil layer (95 cm below the terrace surface) with a radiocarbon age of 4.1–3.7 cal ka BP, suggesting sediment aggradation above previous floodplain levels. As a result, it is likely that the terrace sediment may not have been completely shielded until terrace formation. We do not add an initial concentration to the terrace column model because we largely do not know the ^{14}C concentrations and burial history of the terraces. Any antecedent ^{14}C will increase the concentration of ^{14}C derived from the terraces, so terrace migration rates estimated from our model will be minimum rates.

3.4 | Methods for calculating erosion rates from sediment fluxes

Erosion rates derived from ^{14}C concentrations in catchments with abundant paraglacial terraces are not expected to represent true 'basin-wide' denudation rates. To further understand the relationships between denudation rates and the isostatic uplift rate in these basins, we calculate erosion rates from sediment fluxes. That is, we test whether the erosion rate from sediment fluxes is, in fact, comparable to the isostatic uplift rate in basins with paraglacial terraces when both the 'background' erosion of hillslopes and the erosion of paraglacial material are considered. The erosion rate from sediment flux, E_{flux}, is the sum of the 'background' erosion rate (E_{bg}, units m/year) and of the terrace volume that collapses into the river during a large flood event divided by the sample's drainage area (A in m^2). The latter represents the equivalent erosion rate had the volume of material from the terrace been sourced from uniform erosion upstream of the sample. The volume of sediment from the terraces is the product of the migration distance (D_T in meters), the height of the terrace bank relative to the channel (H_T in meters) and the length of the eroded terrace (L_T in meters; see Section 4 for a full description of these parameters). For the purpose of this study, we assume that terrace collapse occurs during large annual flood events. The erosion rate from sediment flux, in units m/year, is given by the following:

$$E_{flux} = E_{bg} + \frac{L_T H_T D_T}{A} \tag{11}$$

4 | RESULTS

4.1 | Overview of inferred denudation rates

The following section presents catchment-averaged denudation rates inferred from concentrations of ^{14}C in detrital sediments. We say 'inferred' because these denudation rates are based on the assumption that concentrations result from steady, spatially homogeneous denudation. We report rates in mm/year, as these rates are perhaps more intuitive than a mass-based denudation rate which represent an equivalent bedrock lowering with a density of 2650 kg/m^3 in the parent material. The denudation rates reported below are calculated using CAIRN (Mudd *et al.*, 2016), which is described in detail in Section 4. We also calculate denudation rates using version 3 of CRONUS (Balco *et al.*, 2008), which are approximately 10% lower than the CAIRN-derived erosion rates (see Table 2).

Overall, the inferred denudation rates are similar for seven out of the nine sampled sites, with rates between 0.442 and 0.612 mm/year. The denudation rate calculated for the high-elevation, low-relief Gaick plateau is 0.478 mm/year (PLAT). Downstream of this sample, the river flows through a bedrock knickzone (Figure 2) downstream of which the inferred denudation rate is similar to that from the Gaick plateau (sample ADD, 0.442 mm/year). Around 4.5 km downstream, the Feshie then enters the main glacial trough where the main valley-fill sequence begins and debris flows enter the channel. Here, the inferred catchment-averaged denudation rate increases to 0.612 mm/year (UBRU). Further downstream, the denudation rates show little change where the river passes the confluence with the Lorgaidh and flows through the uppermost braided section (UBRM, 0.582 mm/year; FLOD, 0.582 mm/year). The Lorgaidh (LORG), which displays evidence of Holocene hillslope failure (e.g., talus deposits, debris flows) and contains terraces which the river is laterally migrating into, has a slightly lower inferred denudation rate of 0.457 mm/year.

The steep, high-relief Garbhlach tributary has the lowest inferred denudation rate in the entire catchment (GAR, 0.175 mm/year). Downstream of the confluence with the Garbhlach, an inferred denudation rate of 0.523 mm/year is calculated from sample ALEAN which is similar to the sample upstream of the Garbhlach's confluence along the main channel (FLOD, 0.582 mm/year). Finally, our downstream-most sample, MILC, which is ≈ 1.5 km upstream of the Feshie's confluence with the Spey, displays the highest erosion rate recorded in this study, 1.356 mm/year. Overall, the catchment-averaged denudation rates are, on average, significantly lower than the isostatic uplift rates predicted for the Feshie basin of >1 mm/year (Shennan *et al.*, 2009).

Error bars are shown on the CAIRN-derived erosion rates on Figure 7. Error values represent erosion rates calculated from the reported ^{14}C concentrations ± the blank-corrected uncertainty

TABLE 2 ^{14}C sample details, ± blank-corrected ^{14}C concentrations, and modelled erosion rates from CAIRN and CRONUS.

Sample	River name	Lat.	Long.	Basin area (km^2)	Sample elevation (m)	Sample ^{14}C (atoms g $^{-1}$)	Uncertainty ± (atoms g $^{-1}$)	CAIRN-derived erosion rate (mm year $^{-1}$)	CRONUS-derived erosion rate (mm year $^{-1}$)
GAR	Garbhlach	57.03407	−3.8729	4.47	438	100440	2570	0.175	0.167
ADD	Feshie	56.9786	−3.83459	73.13	450	52500	2450	0.442	0.389
LORG	Lorgaidh	57.00016	−3.9047	7.26	376	49050	2500	0.457	0.421
PLAT	Feshie	56.97275	−3.79523	33.57	513	47130	2520	0.478	0.434
ALEAN	Feshie	57.04437	−3.89655	126.57	324	45100	2520	0.523	0.470
FLOD	Feshie	57.02548	−3.89996	116.12	343	42480	2510	0.582	0.514
UBRM	Feshie	57.01004	−3.90527	100.76	358	41290	2510	0.582	0.541
UBRU	Feshie	56.9946	−3.8914	91.65	380	40860	2510	0.612	0.550
MILC	Feshie	57.12184	−3.90915	232.28	229	24260	2520	1.356	1.03

Note: All erosion rates are calculated using the Lal/Stone scaling. We refer the reader to Supporting Information Tables S4 and S5 for more detailed descriptions of the ^{14}C concentrations and erosion rates.

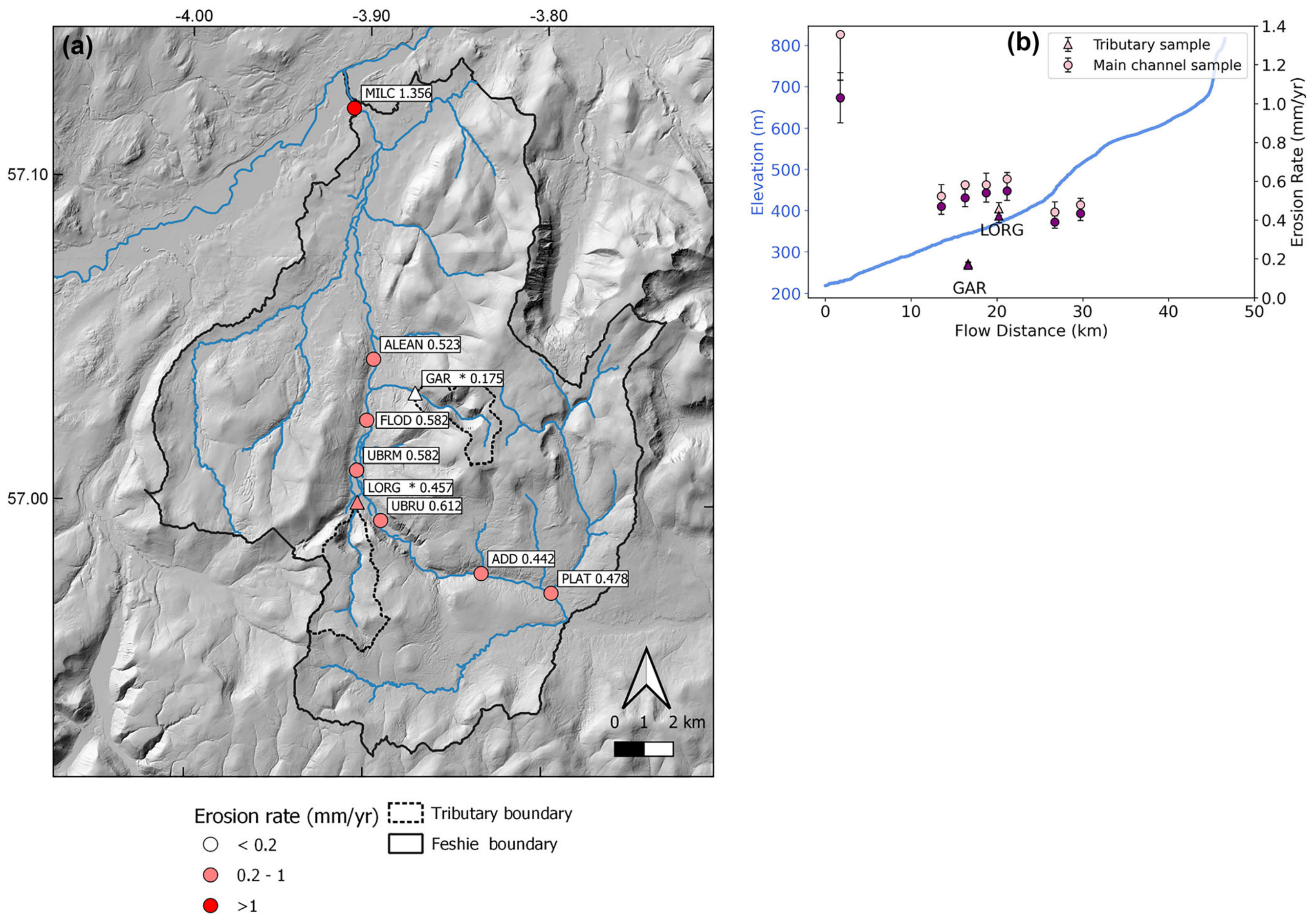

FIGURE 7 (a) Map of the Feshie with sample names and ^{14}C-derived erosion rates. (b) Plot of main river profile (blue line) and erosion rates calculated through both CAIRN (pink markers) and CRONUS (purple markers). CAIRN error values represent erosion rates calculated from the reported ^{14}C concentrations ± the blank-corrected uncertainty values. CRONUS error values represent both measurement uncertainty and production rate uncertainty. We refer the reader to Supporting Information Tables S4 and Table S5 for more detailed descriptions of the ^{14}C concentrations and erosion rates.

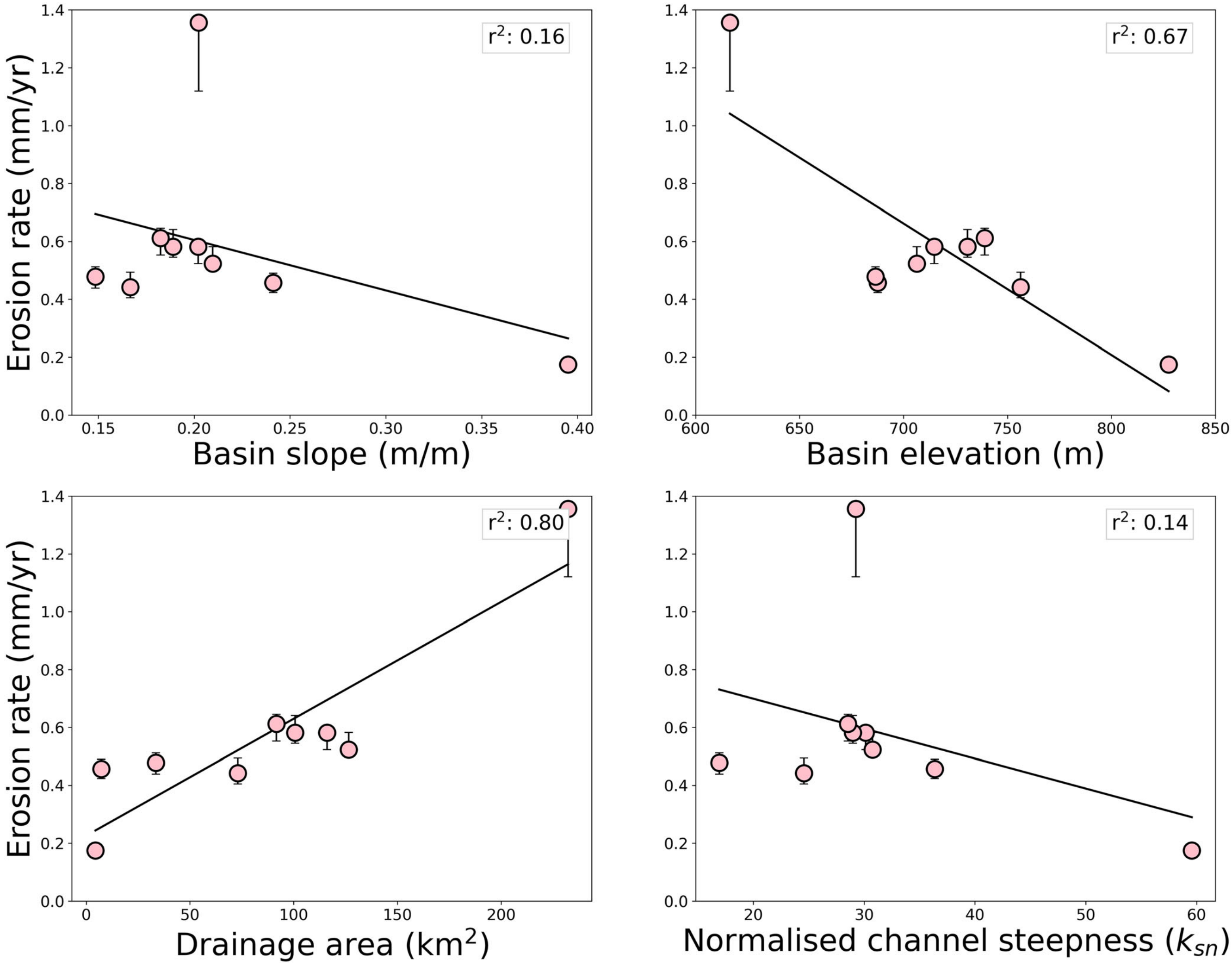

FIGURE 8 Relationship between denudation rates and catchment-averaged topographic parameters including mean basin slope, elevation, drainage area and normalised channel steepness. R^2 linear regression values are shown for each plot.

values. The key findings discussed above remain the same when these errors are considered. That is, we find the lowest inferred denudation in the steep, high-relief Garbhlach tributary and the highest apparent denudation rate at our downstream-most sample near the Spey, MILC. These key findings are also consistent with the denudation rates and uncertainties derived from CRONUS (see Table 2 and Figure 7, Balco *et al*., 2008). We refer the reader to Supporting Information Table S3 for information on blank measurements and uncertainties.

4.2 | Relationships between apparent erosion rates and basin-averaged topographic parameters

Many studies have correlated denudation rates to basin-averaged topographic parameters to understand the wider controls of climate and/or tectonics on landscape evolution (e.g., Cyr *et al*., 2010; Delunel *et al*., 2010; Hack *et al*., 1957; Harel *et al*., 2016; Wittmann *et al*., 2007). In this study, we counter-intuitively find negative correlations between the apparent erosion rates and upstream basin-averaged slope, normalised channel steepness, and elevation (proxy for temperature, Figure 8). We find the highest inferred denudation rate of 1.356 mm/year at the most downstream sample, MILC, and the lowest inferred denudation rate of 0.175 mm/year in the steepest tributary catchment, the Garbhlach basin (GAR). Furthermore, we cannot explain our erosion rates from any apparent geological controls, as the bedrock geology is relatively homogeneous in the catchment (BGS, 2021). Similarly, vegetation does not appear to exert a primary control on the erosion rates. Commercial forestry dominates the lower areas of the catchment near the confluence with the Spey, and new native forest and moorland occupy much of the upper basin. It is important to note that we find the lowest denudation rate in the Garbhlach tributary, a catchment that is very steep and largely devoid of terrace materials. This result supports our hypothesis that a significant portion of the sediment transported by the main stem river is sourced from low-concentration terrace materials. In the following section, we use our mixing model to test this hypothesis.

4.3 | Terrace mixing model results

To run our mixing model, we need a 'background' denudation rate that is representative of catchment-wide denudation. In the absence of other reliable catchment-wide denudation rates, we assume that the Garbhlach's denudation rate of 0.175 mm/year represents this background denudation rate. We note that this is likely an upper bound and that the real background denudation rate may be lower, as the Garbhlach is one of the steepest tributaries in the catchment. Using the GAR value of 0.175 mm/year as the background denudation rate, we use CAIRN to calculate the expected ^{14}C concentration for all the other samples. We then use the mixing model to simulate the impact of introducing lower concentration material from the upstream terraces, as explained in the methods. The dilution proceeds iteratively. For example, the sample near the Spey (MILC) features the lowest ^{14}C concentration and the highest apparent erosion rate (1.356 mm/year). This means that sediments with relatively low ^{14}C concentrations must have been supplied between MILC and ALEAN. The model assumes these lower concentration sediments have been supplied by terraces. We also note that no other potential sources of lower concentration sediments (e.g., landslides) are observed between MILC and ALEAN. The height and age of the terrace will affect the ^{14}C concentrations in the terrace material that is remobilised. For example, erosion of higher and/or younger terraces will lead to the introduction of material with lower average ^{14}C concentrations. The terrace migration rate will affect the ratio of background material to terrace material in the river sediment: the greater the migration rate, the greater the dilution of the background sediment with low ^{14}C concentration sediment from the terraces. We examine each of these possibilities in the following discussion.

4.3.1 | Terrace height results

Figure 9 shows a map and longitudinal river profile of the left and right terrace heights in the Feshie basin. Terrace heights, derived from the 10 m buffer zone, average 2.2 m above the channel for the entire basin (see Figure S5 in the Supporting Information for distribution of terrace heights). There is no obvious downstream trend in terrace heights, although terraces in the headwaters (upstream of flow distance 35 km) tend to be not as high as further downstream. Localised reaches with higher terraces above ≈5 m are observed at locations such as the Garbhlach confluence and upstream of sample UBRU (flow distance between 20 and 25 km). Terrace heights do not appear to increase between sample ALEAN and MILC, and average between 2 and 2.5 m, suggesting that terrace height does not account for the higher erosion rate (lower concentration) near the Spey. There do not appear to be any high terraces feeding the tributary channels between ALEAN and MILC.

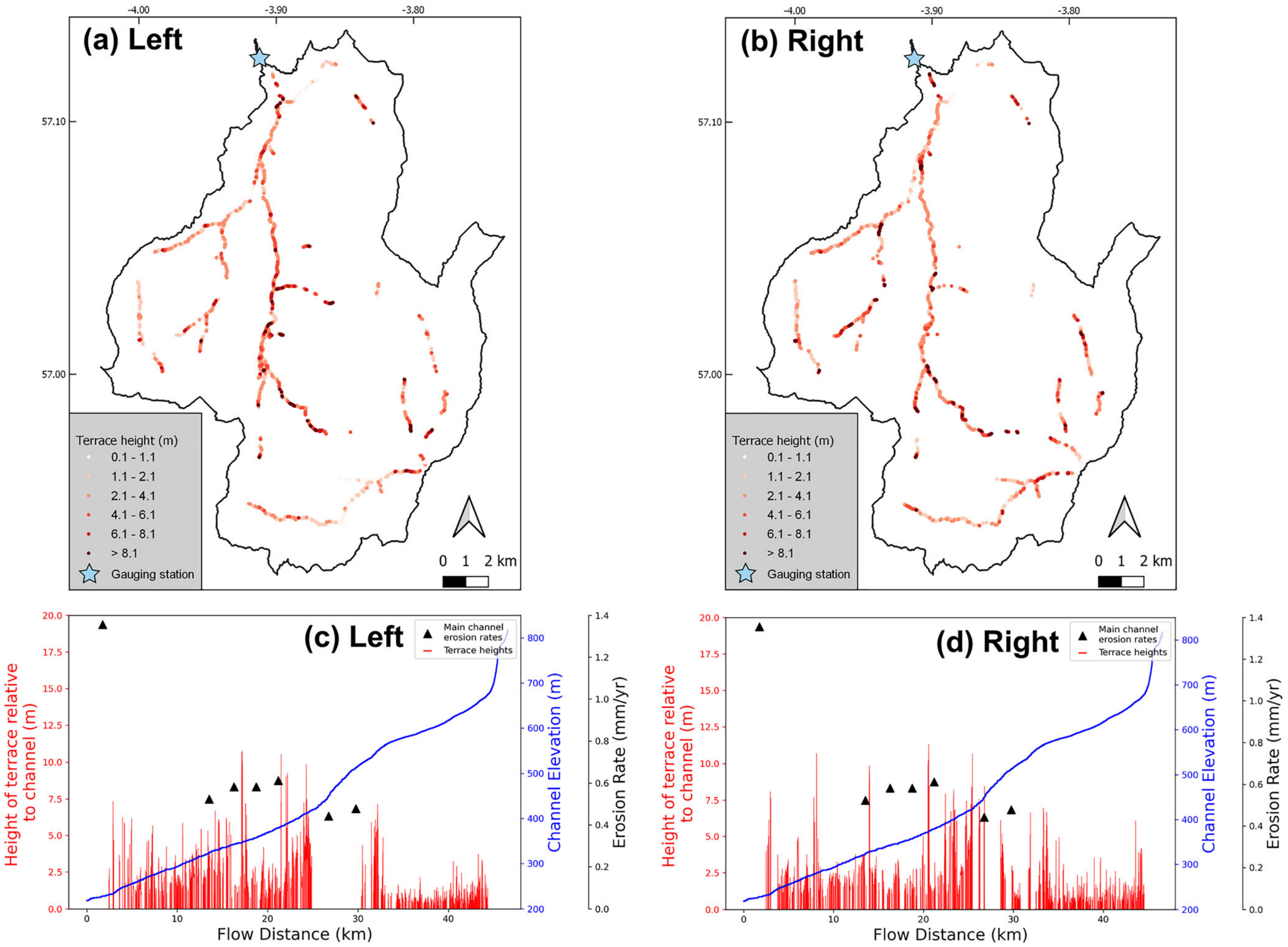

FIGURE 9 (a, b) Maps of left (a) and right (b) terrace heights (m) derived from the 2009 flood with a 10-m buffer. (c, d) Long profile plot of the main Feshie River with left (c) and right (d) terrace heights marked in red. Main channel erosion rates are shown by the black triangles.

4.3.2 | Terrace age results

Figure 10 shows the relationship between terrace ages and depth-averaged ^{14}C concentrations for the average terrace height of 2.2 m and average terrace elevation of 420 m in the Feshie basin, simulated by our terrace column model. As the average terrace age increases, the depth-averaged terrace ^{14}C concentration increases.

Terrace elevations mostly range between 230 and 600 m, which is ≈200 m below and above the mean elevation of 420 m in the Feshie basin. With regard to the influence of elevation on ^{14}C production rates, a change in terrace elevation of 200 m changes the final terrace concentration by 10% for our average terrace height of 2.2 m. Error bars on Figure 10 represent this 10% uncertainty (see Table S2 in the Supporting Information for full sensitivity analysis). Latitude makes a negligible difference to the modelled terrace concentrations due to the catchment size. The uncertainty from elevation on terrace ages is discussed in more detail alongside the terrace migration results in Section 4.

As discussed in Section 4, Robertson Rintoul (1986) interpreted the lower level terraces in the Feshie basin to have formed 1000 (Group 4) and 4000 (Group 3) years ago, from radiocarbon dating and geomorphic mapping. These ages correspond to depth-averaged terrace ^{14}C concentrations of approximately 8000 and 27 000 atoms/g, respectively. Therefore, we tentatively model each samples' ^{14}C basin outlet concentration with terrace migration distances associated with these depth-averaged terrace concentrations and discuss the implications in Section 4.

4.3.3 | Terrace migration distance results

We first present results using a range of catchment-averaged terrace migration distances per flood event (D_T in Equation (9)), that is, all terraces upstream of each sampling point are assumed to migrate at the same rate. We perform the calculation for each sampling point. The results for ALEAN and MILC (sample near Spey) are shown in Figure 11. The remainder of the samples yield similar results to ALEAN and are shown in Figure S6 in the Supporting Information. If the terraces that are contributing sediment to the modern channel have been exposed to cosmic rays for 1000 years throughout the Feshie basin, then we can explain MILC's lower sampled concentration with higher terrace migration distances during a flood event. This result remains valid even when we take into account the uncertainty from terrace elevation-derived production rates (see shaded lines on Figure 11). For example, if the average terrace concentrations in the Feshie equate to 8000 atoms/g (i.e., exposed to cosmic rays for 1000 years), then we can explain ALEAN's observed basin outlet concentration with catchment-averaged terrace migration distances of 0.08 m/flood event. To explain the highest apparent erosion rate from the MILC sample (with the lowest measured ^{14}C concentration) downstream near the Spey, catchment-averaged terrace migration distances must be significantly higher (0.3 m/flood event) for the same terrace concentration of 8000 atoms/g.

The terrace migration values presented above are catchment-averaged. However, we know that the sediment sampled at ALEAN has a ^{14}C concentration that is nearly twice that at MILC further downstream, implying that a significant change in terrace dynamics occurs in the nested basin between ALEAN and MILC. Major rivers within this nested basin include both the section of the main Feshie channel between the two sampling locations and the Fhearnasdail tributary (see Figure 1 for location). To calculate the required migration distances in this nested basin, we run our sediment mixing model (Equation (9)) and set the terrace migration distances upstream of ALEAN to 0.08 m/flood event (e.g., 1000-year scenario). We then model the required nested basin's terrace migration distances to obtain MILC's outlet concentration. For example, if the terraces upstream of ALEAN have a migration rate of 0.08 m/flood event, we find that the nested basin requires migration distances of around 0.5 m/flood event if terraces have been exposed to cosmic rays for 1000 years.

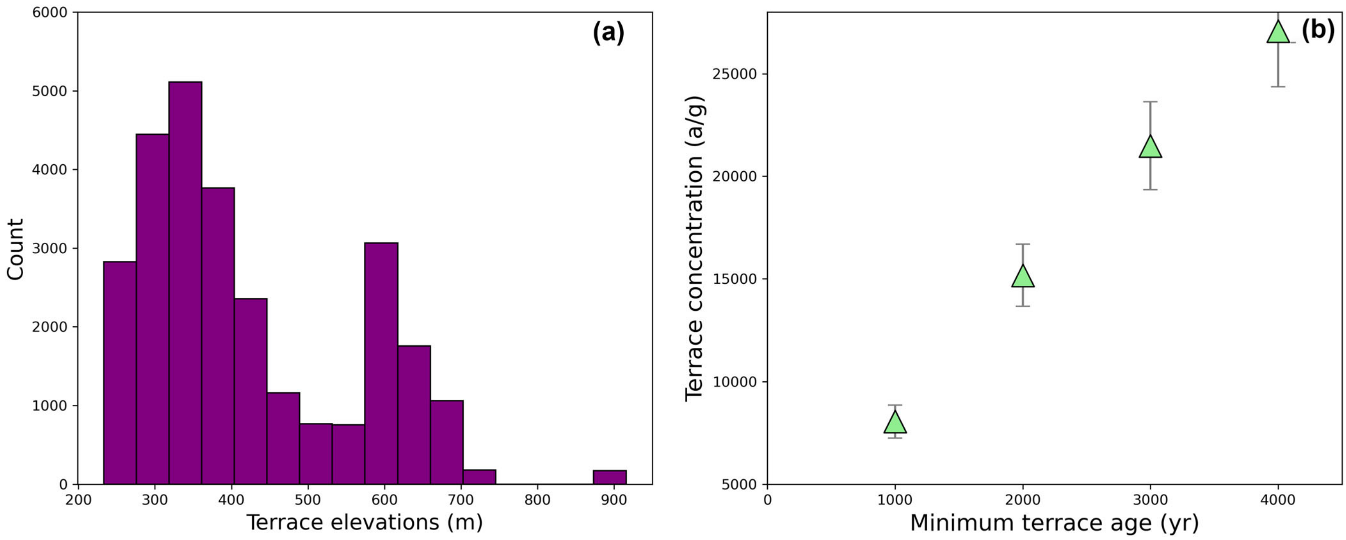

FIGURE 10 (a) Histogram of the terrace elevations derived from the 10-m buffer method for the entire Feshie catchment. (b) Relationship between terrace age and depth-averaged terrace ^{14}C concentration using our average terrace height of 2.2 m and elevation of 420 m. 10% error bars represent uncertainty associated with the production rates from terrace elevation (i.e., an increase in elevation of 200 m increases the terrace ^{14}C concentration by approximately 10% for the same terrace scarp height).

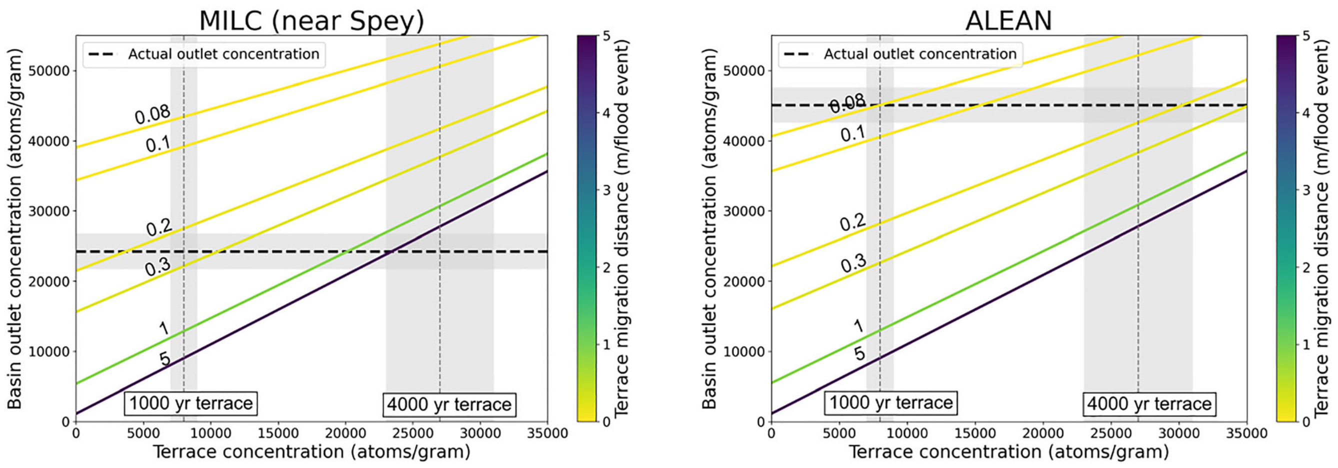

FIGURE 11 Results of the mixing model for MILC (downstream site near Spey) and ALEAN. This model considers catchment-averaged terrace migration rates, that is, all terraces upstream of each sampling location migrate at the same rates. The measured ^{14}C concentration at these sites ('actual outlet concentration') is shown by the black horizontal dashed line. Blank-corrected analytical uncertainties are shown by the grey shaded error bars on the 'actual outlet concentration'. The influence of various terrace migration distances per flood event (0.08, 0.1, 0.2, 0.3, 1, 5 m) on the predicted ^{14}C concentration at these sites is shown by the coloured lines with their corresponding terrace concentrations. Grey vertical lines represent concentrations for terrace with ages of 1000 (8000 atoms/g) and 4000 years (27 000 atoms/g), with shaded 10% error bars. These error bars represent uncertainty from terrace elevation-derived ^{14}C production rates (see Section 4). See Figure S6 in the Supporting Information for results at other sample sites.

Another hypothesis is that the terraces in the Feshie basin have been exposed to cosmic rays for 4000 years and thus have an approximate depth-averaged ^{14}C concentration of 27 000 atoms/gram (see Section 4). In this scenario, terraces upstream of ALEAN require a basin-averaged retreat rate of approximately 0.2 m/flood event. Our results suggest that it may be possible to yield MILC's lower basin outlet concentration with basin-averaged retreat rates of 5 m/flood event when considering terrace production rate uncertainties. However, we know that, in this scenario (i.e., terraces exposed to cosmic rays for 4000 years), the required migration distances upstream of ALEAN are 0.2 m/flood event. When we calculate the required terrace migration rates in the nested basin between MILC and ALEAN, we find that even a terrace migration rate of 1000 m/flood event, which is unrealistic, cannot yield the measured outlet concentration at MILC. We therefore cannot explain MILC's basin outlet concentration if all terraces that are feeding material into the modern channel have relatively high ^{14}C concentrations (i.e., 27 000 atoms/gram).

An alternative hypothesis to the lower concentration recorded at MILC is the possibility of younger terraces between MILC and ALEAN that are inputting lower concentration material into the river. Our basin-averaged terrace model suggests that the lower basin outlet concentration at MILC could be explained if MILC has younger catchment-averaged terraces than ALEAN, while the terrace migration rates remain the same (Figure 11). That is, if terraces upstream of ALEAN have been exposed to cosmic rays for 4000 years (i.e., terrace group 3 according to Robertson Rintoul (1986)'s classification), then a terrace migration rate of 0.2 m/flood event is required. Likewise, if terraces in the entire MILC basin have been exposed to cosmic rays for 1000 years (terrace group 4), then a similar terrace migration rate of 0.2 m/flood event can explain the lower basin outlet concentration. However, we know that, in this scenario, terraces upstream of ALEAN have a depth-averaged ^{14}C concentration of 27 000 atoms/gram (i.e., exposed to cosmic rays for 4000 years), which means that the nested basin between ALEAN and MILC is where a change in terrace concentrations must occur if the retreat rates remain the same. If we run our mixing model and set the terraces upstream of ALEAN to 27 000 atoms/gram, we find that even if the terraces in the nested basin have a ^{14}C concentration of 0 atoms/gram, then MILC's basin outlet concentration cannot be obtained. Therefore, younger terrace ages alone cannot account for MILC's basin outlet concentration as it is not possible to obtain the outlet concentration at MILC with the same migration distances as ALEAN.

4.4 | Erosion rates from sediment fluxes

Here, we present overall sediment volumes sourced from both paraglacial terraces and 'background' material on annual timescales (Figure 12). Specifically, we assume that terrace material is sourced from large annual flood events and that the 'background' denudation rate is that of the Garbhlach's, 0.175 mm/year, for the entire Feshie basin. The volume of sediment from the terraces is the product of the migration distance (D_T), the height of the terrace banks relative to the channel (H_T) and the length of the eroded terraces (L_T). Regarding the terrace migration distances, we use the basin-averaged migration distances associated with a 1000-year-old terrace for each sample (see Section 4). We use this scenario because we can obtain realistic terrace migration rates when we mix the 'background' sediment with 1000-year-old terraces that, importantly, have low ^{14}C concentrations. We do not use migration rates associated with 4000-year-old terraces because the modelled concentrations in these terraces are higher and require unrealistic migration rates (see Figure 11).

The total volume of sediment sourced from paraglacial terraces during large annual flood events is slightly lower than the 'background' sediment volume for most samples (Figure 12). MILC, which is the sample located near the confluence with the Spey and has the lowest basin outlet ^{14}C concentration, has a significantly higher terrace volume relative to the 'background' volume. That is, to explain

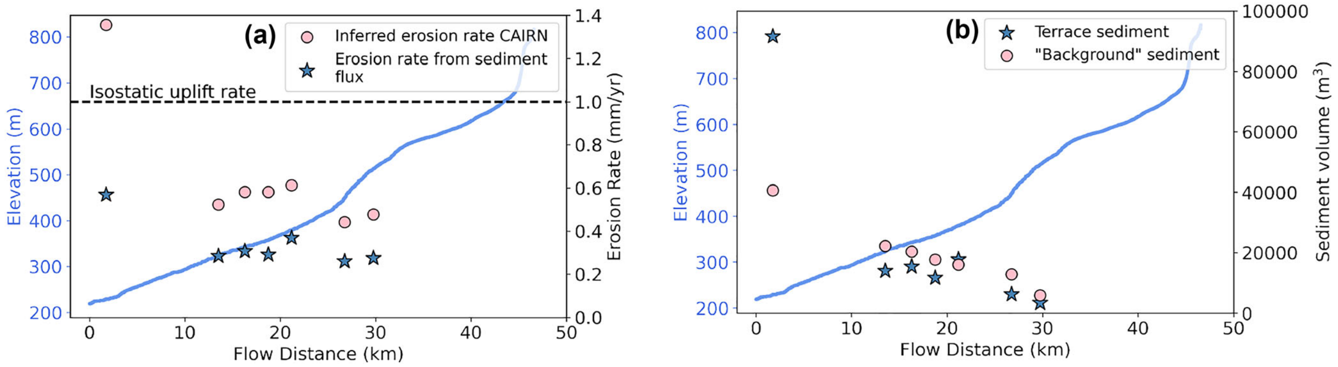

FIGURE 12 (a) CAIRN erosion rates and sediment flux erosion rates for main channel samples. Sediment flux erosion rates represent the sum of the 'background' erosion rates and the terrace erosion rates. The approximate isostatic uplift rate is marked by a black dashed line (Shennan *et al.* 2009). (b) Paraglacial terrace and 'background' sediment volumes for main channel samples. The background denudation rate (from CAIRN) for the Garbhlach basin, 0.175 mm/year, was used to calculate the 'background' sediment volumes and sediment flux derived erosion rates shown in these plots. Terrace migration rates associated with a terrace age of 1000 years were used to calculate terrace volumes and erosion rates from sediment fluxes.

MILC's low outlet concentration, we need to dilute the 'background' concentration with a larger volume of low concentration terrace material compared to the other samples which require smaller terrace volumes (due to their higher basin outlet concentrations).

We calculate erosion rates from sediment fluxes in basins with abundant paraglacial terraces (i.e., all samples except GAR). Similar to the inferred erosion rates from CAIRN, we find that these erosion rates are significantly lower than the isostatic uplift rates for the Feshie basin.

5 | DISCUSSION

5.1 | Relationships between uplift, denudation and slope

We interpret the Garbhlach's denudation rate of 0.175 mm/year to be representative of the true catchment-wide denudation because unlike the remainder of our sampled basins, the Garbhlach is largely devoid of transient sediment stores and the hillslopes in the Garbhlach basin appear to be connected to the channel, as shown by the 'V'-shaped valley. The Garbhlach's denudation rate is near the upper bound of previously reported Late Holocene bedrock incision rates in upland rivers in Scotland. Jansen *et al.* (2011) and Kim (2004) inferred the present-day vertical incision rates of 0.07–0.24 mm/year by measuring ^{10}Be concentrations of bedrock surfaces along knickpoint reaches that are assumed to be caused by base-level fall. The Garbhlach is also the steepest catchment in the Feshie basin which supports the idea that 0.175 mm/year is likely to be an upper bound and that the real background denudation rate in the Feshie may be lower. Nonetheless, the Garbhlach's denudation rate is an order of magnitude lower than the glacial isostatic uplift rates predicted for the Feshie basin of >1 mm/year (Shennan *et al.*, 2009). We also find that erosion rates calculated from sediment fluxes, which represent the sum of the 'background' and terrace erosion rates and vary between 0.2 and 0.6 mm/year, are lower than the isostatic uplift rate. These results support studies which have proposed that base-level signals propagating inland from the coast, which are indicated by the presence of knickpoints, have stagnated near Scotland's coastlines (Bishop *et al.*, 2005; Castillo *et al.*, 2013). Likewise, we also find that the inferred denudation rates (0.175–1.356 mm/year) do not correlate with any basin-wide topographic characteristics, such as the normalised channel steepness index. Our findings therefore align with studies which have suggested that without the renewal of relief through sustained tectonic activity or base-level lowering, post-glaciated landscapes in tectonically quiescent terrains may remain in a state of transient dynamics that last for millions of years (e.g., Ballantyne, 2002; Egholm *et al.*, 2013; Whitbread *et al.*, 2015). In the absence of sustained tectonic uplift, valleys are likely to maintain their glacially inherited 'U'-shaped topography, meaning hillslopes will remain largely decoupled from channels.

5.2 | Variations in the spatial distribution of the inferred denudation rates

To explain the spatial distribution of our inferred denudation rates, we suggest catchments with paraglacial terraces, into which the rivers are actively eroding (inferred from flood modelling, geomorphic mapping and remote sensing observations), record apparently higher CRN denudation rates in comparison to catchments with little alluvial fill. The novel sediment mixing model presented can reproduce basin outlet ^{14}C concentrations that correlate to those observed in ^{14}C measurements, using terrace heights, lengths and realistic terrace migration distances. Thus, we interpret paraglacial terraces to be a primary source of sediment in the Feshie River which supports previous studies (Robertson Rintoul, 1986; Young, 1976) and highlights the long-lasting impact of the glacial legacy.

Our interpretation of ^{14}C-derived denudation rates to not reflect basin-wide denudation in catchments with significant sediment storage aligns with theoretical and recent applied ^{14}C studies (e.g., Hippe, 2017; Slosson *et al.*, 2022). For example, Slosson *et al.* (2022) attributed the relatively lower concentrations of ^{14}C in comparison to ^{10}Be concentrations in their study area in the Andes to the presence of complex sediment storage dynamics in hillslope deposits. Future studies should therefore carefully characterise upstream geomorphic processes when using ^{14}C to infer denudation rates, as ^{14}C concentrations appear highly sensitive to such processes due to the relatively short timescales over which ^{14}C accumulates and decays.

In our mixing model, we assume that the Garbhlach's denudation rate of 0.175 mm/year represents the 'background' denudation rate because the Garbhlach is largely devoid of transient sediment stores. As mentioned previously, we believe that this rate of 0.175 mm/year is likely to be an upper bound as the Garbhlach is the steepest tributary catchment in the Feshie basin; the real background denudation rate in the Feshie may be lower. We find that lowering the 'background' denudation rate in our mixing model makes a minor difference to the terrace migration rates (see Figure S7 in the Supporting Information). A future research direction therefore includes sampling across a range of slope gradients where the upstream basins are devoid of sediment stores.

Studies have shown that CRN-derived erosion rates based on samples of a given grain size fraction (e.g., sand) may not give a complete picture of the denudation of the surrounding hillslopes, as sediment of different grain size fractions may experience different denudation histories: sand may originate from the abrasion of clasts during fluvial transport, whereas larger clasts may originate from processes such as deep-seated landslides (e.g., Belmont *et al*., 2007; Lupker *et al*., 2017). This may challenge the interpretation of the GAR sample (0.175 mm/year) which is assumed to represent basin-wide denudation. However, field observations of hillslope material in the Garbhlach basin show abundant sand in soils within hillslope material and debris flows (see Figure S8 in the Supporting Information), due to the granite weathering by granular disintegration in this climate. This observation suggests that the sand sampled in the Garbhlach is representative of surrounding hillslope erosion from debris flows and plateau erosional processes. Extracting ^{14}C concentrations from the pebble fraction would shed further light on this theory.

5.3 | Terrace migration and terrace ages in Scottish rivers

The modelled terrace migration distances presented in Section 4 are basin-averaged (and nested basin-averaged); that is, the model assumes that all terraces connected to the channel at high flow erode at the same rate. The migration rates we have calculated appear reasonable for such an active river, which is a characteristic feature of the Feshie (e.g., Ballantyne, 2019; Rumsby *et al*., 2008; Williams *et al*., 2020). We found that terrace migration rates between 0.08 and 0.5 m per flood event are required to explain our measured ^{14}C concentrations. However, it is unlikely that terraces migrate at the same rate across the catchment: The values we derived may instead represent an average that reflects a mix between sections that erode slowly and terrace reaches that experience large amounts of geomorphic change locally. For example, through flood modelling, Fieman *et al*. (2020) did not observe widespread change in the channel planform along the 140 km long River Dee, Aberdeenshire, following Storm Frank (>200 year recurrence interval). Instead, they observed meter-scale change at the reach scale (1 km). Our results show that to obtain MILC's basin outlet concentration, the terrace migration distances must be higher between the MILC and ALEAN sampling locations, even when taking into account production rate uncertainties and terrace age variations. This supports the idea that significant geomorphic changes may occur locally, as exemplified by the 5-km reach downstream of the confluence with the Fhearnasdail tributary. Satellite imagery observations show this reach to be exceptionally braided with tens of meters of bank migration observed between 2006 and 2019 (Figure 3). Repeat topographic surveys and bank inundation modelling would shed light on the spatial distribution, timing and frequency of terrace erosion (e.g., Williams *et al*., 2016; Williams *et al*., 2020).

The mixing model presented in Equation (9) assumes that the total height of a terrace column collapses into the river during a flood event. It is likely, however, that not all terraces eroded through total column collapse during the flood event before sample collection. That is, some terraces may have eroded by undercutting alone, meaning that only their base was eroded, while others may have eroded from top collapse, due to destabilisation of the base from previous flood events. If we consider a scenario where all three mechanisms of terrace collapse occur throughout the Feshie basin, then the average concentration of ^{14}C coming from the terraces will be similar to a scenario where we only consider total column collapse. For example, if terraces in the Feshie formed 1000 years ago and have an average total height of 2.2 m, with one third eroding due to undercutting (e.g., depth from surface = 1.1 to 2.2 m, average terrace concentration = 4000 atoms/g), one third eroding from the terrace top collapsing (e.g., depth from surface = 0 to 1.1 m, average terrace concentration = 12000 atoms/g) and one third eroding based on total terrace thickness (e.g., average terrace concentration = 8000 atoms/g), then the average terrace concentration (8000 atoms/g) is the same as concentrations from the terrace erosion model based on the total terrace column thickness alone. In addition, a combination of terrace erosion mechanisms (i.e., undercutting, top collapse, and total column collapse) would also mean that the average terrace height in Equation (9) would be lower than a scenario where we just consider the whole terrace column collapsing. The basin average terrace retreat rates would therefore be higher in a scenario where terraces erode by various mechanisms.

A future research direction includes constraining the concentrations of paraglacial terraces in the Feshie basin, which would shed light on their ages and burial history. Designing a sampling strategy to correlate preserved terraces by terrace height (relative to the channel) appears challenging, however. Field observations of bedrock reaches (e.g., bedrock knickzone marked on Figure 2, bedrock reach at the bridge downstream from sample ALEAN) between alluvial reaches suggests terraces could be longitudinally disconnected. This means that inferring basin-wide terrace ages (from a small number of sampled terrace profiles) by terrace heights requires careful consideration of the aforementioned geographical, morphological and temporal complexities.

In the terrace column model, we assume there is no initial ^{14}C concentration, on the basis that the material was buried deep enough before the formation of the terrace such that all pre-existing ^{14}C had decayed. There is a strong possibility that the terraces contain more ^{14}C than considered in our end-member scenario, as suggested by the presence of 4 ka old charcoal fragments buried within a terrace, which suggests that sediment was transported and deposited 4 ka ago (Robertson Rintoul, 1986)). As such, the terrace migration rates estimated from our experiment will be minimum rates. As discussed in the previous paragraph, we highlight the dating of terraces in the Feshie basin as a future research direction.

5.4 | Choice of CRN to infer denudation rates in post-glacial landscapes

The average integration timescale of the denudation rate for the Garbhlach basin is approximately 3400 years (Lal, 1991). According to this integration timescale, it could be possible to constrain denudation rates with ^{10}Be in high-relief basins with complex Late Pleistocene glacial histories. However, it is important to consider that the erosion rates and integration timescales are catchment averaged and that in reality, a basin will very rarely erode uniformly; some areas will undergo faster denudation, while others will erode more slowly. Regarding the Garbhlach basin, it is likely that its upper reaches, which drain the low-relief Cairngorm plateau (see Figure 1), erode at a lower rate than the catchment-averaged rate and potentially integrate over the Late Pleistocene. For example, denudation rates lower than approximately 0.05 mm/year would integrate over the Late Pleistocene, when the Feshie catchment may have been glaciated (Chandler *et al*., 2019; Sissons, 1974)). The long half-life of ^{10}Be (1.39 Myr) relative to ^{14}C (5700 years) means that ^{10}Be would contain larger amounts of uncertainty from prior exposure during interglacial and interstadial periods. The short half-life of ^{14}C means that inferred denudation rates from ^{14}C atoms in stream sediments will mainly reflect Holocene denudation rates and sediment storage dynamics. ^{14}C is therefore particularly useful for understanding landscape evolution in regions with complex Pleistocene glacial histories. Moreover, sediment grains in glacial and paraglacial deposits (e.g., till, paraglacial terraces), which we suggest contribute to the modern channel sediment flux, may have been transported across topographic divides with different glacial histories. Understanding the inherited component of ^{10}Be (due to its long half-life) in these sediment stores is challenging.

6 | CONCLUSIONS

In this study, we calculate Scotland's first denudation rates over late Holocene time scales from ^{14}C concentrations in stream sediments. We counter-intuitively find that the inferred denudation rates (0.175–1.356 mm/year) do not correlate with any basin-wide topographic characteristics (e.g., slope) and are, on average, lower than the glacial isostatic uplift rates predicted for the Feshie basin of >1 mm/year.

We find that catchments with paraglacial terraces into which the rivers are actively eroding (inferred from field observations, flood modelling and geomorphic mapping) record higher apparent CRN denudation rates in comparison to catchments with little alluvial fill. Terraces are expected to deliver lower concentration material because the production of CRN in terrace materials decreases with surface depth and terraces were buried until the last phase of major Holocene incision (post-4000 years). The steepest tributary catchment of the Feshie River, the Garbhlach, which is largely devoid of terraces, records an apparent denudation rate of 0.175 mm/year, providing an upper bound on the background erosion rate in the Feshie. We propose that the higher apparent denudation rates along the main stem of the Feshie River and the Lorgaidh tributary result from the mixing of 'background' sediment with low-CRN-concentration material derived from terrace erosion. These results suggest that ^{14}C-derived denudation rates in catchments with paraglacial terraces are not representative of true catchment-averaged denudation rates because the ^{14}C concentrations can be influenced by short-lived sediment routing and storage processes due to the isotope's short half-life (5700 years).

We present a sediment mixing model which combines the 'background' sediment from catchment-wide denudation with sediment derived from the incision of paraglacial terraces. We model terrace migration distances during major flood events and calculate the ^{14}C concentration at each sampling location using two terrace age scenarios (1000 and 4000 years old). We demonstrate that the samples from the upper and middle sections of the Feshie basin require similar catchment-averaged terrace migration distances of 0.08 m/flood event (1000-year old terraces) to produce the observed ^{14}C concentrations, when considering a flood event with a return period of around 5 years. We show that the lower area of the Feshie basin requires higher terrace migration distances (e.g., 0.5 m/flood event for the area between ALEAN and MILC for 1000 year scenario) to obtain the measured ^{14}C concentration at the downstream-most sampling site. These rates are compatible with terrace migration rates derived from satellite imagery between 2006 and 2019. These novel results highlight the long-lasting impacts of the glacial legacy on sediment dynamics and indicate that future studies should carefully characterise upstream geomorphic processes when using ^{14}C to infer denudation rates.

ACKNOWLEDGEMENTS

A.H.T. was funded by a NERC Doctoral Training Partnership Grant (NE/S007407/1), with further support from the Scottish Environmental Protection Agency. We would like to thank Elizabeth H. Dingle who helped with field data collection. We would also like to thank two anonymous reviewers and the Associate Editor for thoughtful comments and feedback that have helped to improve the paper.

CONFLICT OF INTEREST STATEMENT

The authors declare that there are no conflicts of interest.

AUTHOR CONTRIBUTIONS

a. Conceptualisation: Anya H. Towers, Simon M. Mudd, Mikael Attal, Fiona J. Clubb
b. Funding acquisition: Anya H. Towers, Simon M. Mudd, Mikael Attal, Fiona J. Clubb
c. Methodology:
    - 14C extraction and AMS measurements: Steve A. Binnie, Tibor J. Dunai, Negar Haghipour
    - Topographic analysis: Anya H. Towers, Simon M. Mudd, Mikael Attal, Fiona J. Clubb
d. Investigation (data collection): Anya H. Towers, Simon M. Mudd, Mikael Attal, Fiona J. Clubb
e. Resources (provision of data): Anya H. Towers, Simon M. Mudd, Mikael Attal, Fiona J. Clubb, Steve A. Binnie, Tibor J. Dunai, Negar Haghipour
f. Software: Anya H. Towers, Simon M. Mudd
g. Supervision: Simon M. Mudd, Mikael Attal, Fiona J. Clubb
h. Writing (initial draft): Anya H. Towers, Simon M. Mudd, Tibor J. Dunai

i. Writing (reviewing and editing): Anya H. Towers, Simon M. Mudd, Mikael Attal, Fiona J. Clubb, Steve A. Binnie, Tibor J. Dunai

DATA AVAILABILITY STATEMENT

All data used in this paper are available upon request. The code for CAIRN and the terrace column model was written by S.M.M. and can be freely accessed at https://github.com/LSDtopotools/.

ORCID

Anya H. Towers https://orcid.org/0009-0005-7409-8869

REFERENCES

BGS (2021) British geological survey: bedrock and superficial maps. Available from: https://digimap.edina.ac.uk/ [Accessed June 2015].

Bailey, F.E. & Koleske, J.V. (1990) *Alkylene oxides and their polymers*, 1. Dekker: New York.

Balco, G., Stone, J.O., Lifton, N.A. & Dunai, T.J. (2008) A complete and easily accessible means of calculating surface exposure ages or erosion rates from 10Be and 26Al measurements. *Quaternary Geochronology*, 3(3), 174–195.

Ballantyne, C.K. (2002) A general model of paraglacial landscape response. *Holocene*, 12(3), 371–376.

Ballantyne, C.K. (2019) After the ice: lateglacial and holocene landforms and landscape evolution in Scotland. *Earth and Environmental Science Transactions of the Royal Society of Edinburgh*, 110(1-2), 133–171.

Ballantyne, C.K., Hall, A.M. & Dawson, A.G. (2021) The quaternary in Scotland. In *World geomorphological landscapes*, Springer Science and Business Media B.V.; 53–96.

Belmont, P., Pazzaglia, F.J. & Gosse, J.C. (2007) Cosmogenic 10Be as a tracer for hillslope and channel sediment dynamics in the Clearwater River, Western Washington State. *Earth and Planetary Science Letters*, 264(1), 123–135. Available from: https://www.sciencedirect.com/science/article/pii/S0012821X07005717

Beven, K. (1997) TOPMODEL: a critique. *Hydrological Processes*, 11(9), 1069–1085.

Bierman, P.R. (1994) Using in situ produced cosmogenic isotopes to estimate rates of landscape evolution: a review from the geomorphic perspective. *Journal of Geophysical Research* 99(B7).

Bing Maps (2023) Bing maps. Available from: https://www.bing.com/maps/ [Accessed July 2023].

Binnie, S.A., Dewald, A., Heinze, S., Voronina, E., Hein, A., Wittmann, H., von Blanckenburg, F., Hetzel, R., Christl, M., Schaller, M., Lanni, L., ASTER Team, Hippe, K., Vockenhuber, C., Ivy-Ochs, S., Maden, C., Fp, R.-H., Fink, D., Wilcken, K.M., Fujioka, T., Fabel, D., Freeman, S. P. H.T., Xu, S., Fifield, L.K., Akar, N., Spiegel, C. & Dunai, T.J. (2019) Preliminary results of CoQtz-N: a quartz reference material for terrestrial in-situ cosmogenic 10Be and 26Al measurements. *Nuclear Instruments and Methods in Physics Research Section B: Beam Interactions with Materials and Atoms*, 456, 203–212. Available from: https://www.sciencedirect.com/science/article/pii/S0168583X19302575

Bishop, P., Hoey, T.B., Jansen, J.D. & Lexartza Artza, I. (2005) Knickpoint recession rate and catchment area: the case of uplifted rivers in Eastern Scotland. *Earth Surface Processes and Landforms*, 30(6), 767–778.

Bodnar, R.J., Binns, P.R. & Hall, D.L. (1987) Synthetic fluid inclusions - VI. Quantitative evaluation of the decrepitation behaviour of fluid inclusions in quartz at one atmosphere confining pressure. *Journal of Metamorphic Geology*, 7(2), 229–242. Available from: https://doi.org/10.1111/j.1525-1314.1989.tb00586.x

Bodnar, Vityk (1984) Interpretation of microthermometric data for H2O-NaCl fluid inclusions. Fluid inclusions in Minerals, Methods and Applications, Vivo and Frezotti (eds) Virginia Tech, 117-130.

Bookhagen, B. & Strecker, M.R. (2012) Spatiotemporal trends in erosion rates across a pronounced rainfall gradient: examples from the southern Central Andes. *Earth and Planetary Science Letters* 327-328: 97–110. Available from: https://doi.org/10.1016/j.epsl.2012.02.005

Borchers, B., Marrero, S., Balco, G., Caffee, M., Goehring, B., Lifton, N., Nishiizumi, K., Phillips, F., Schaefer, J. & Stone, J. (2016) Geological calibration of spallation production rates in the CRONUS-Earth project. *Quaternary Geochronology*, 31, 188–198. Available from: https://doi.org/10.1016/j.quageo.2015.01.009

Braucher, R., Del Castillo, P., Siame, L., Hidy, A.J. & Bourlés, D.L. (2009) Determination of both exposure time and denudation rate from an in situ-produced 10Be depth profile: a mathematical proof of uniqueness. Model sensitivity and applications to natural cases. *Quaternary Geochronology*, 4(1), 56–67.

Brown, E.T., Stallard, R.F., Larsen, M.C., Raisbeck, G.M. & Yiou, F. (1995) Denudation rates determined from the accumulation of in situ-produced 10Be in the Luquillo experimental forest, Puerto Rico. *Earth and Planetary Science Letters*, 129(1-4), 193–202.

Castillo, M., Bishop, P. & Jansen, J.D. (2013) Knickpoint retreat and transient bedrock channel morphology triggered by base-level fall in small bedrock river catchments: the case of the Isle of Jura, Scotland. *Geomorphology* 180-181: 1–9. Available from: https://doi.org/10.1016/j.geomorph.2012.08.023

Chandler, B. M.P., Boston, C.M. & Lukas, S. (2019) A spatially-restricted Younger Dryas plateau icefield in the Gaick, Scotland: reconstruction and palaeoclimatic implications. *Quaternary Science Reviews*, 211, 107–135. Available from: https://doi.org/10.1016/j.quascirev.2019.03.019

Charreau, J., Blard, P.-H., Zumaque, J., Martin, L. C.P., Delobel, T. & Szafran, L. (2019) Basinga: a cell-by-cell GIS toolbox for computing basin average scaling factors, cosmogenic production rates and denudation rates. *Earth Surface Processes and Landforms*, 44(12), 2349–2365.

Chmeleff, J., von Blanckenburg, F., Kossert, K. & Jakob, D. (2010) Determination of the 10Be half-life by multicollector ICP-MS and liquid scintillation counting. *Nuclear Instruments and Methods in Physics Research, Section B: Beam Interactions with Materials and Atoms*, 268(2), 192–199. Available from: https://doi.org/10.1016/j.nimb.2009.09.012

Chow, V.T. (1959) *Open channel hydraulics*. McGraw-Hill Book Co.: New York.

Church, M. & Ryder, J.M. (1972) Paraglacial sedimentation: a consideration of fluvial processes conditioned by glaciation. *Bulletin of the Geological Society of America*, 83(10), 3059–3072.

Clark, C.D., Ely, J.C., Greenwood, S.L., Hughes, A. L.C., Meehan, R., Barr, I.D., Bateman, M.D., Bradwell, T., Doole, J., Evans, D. J.A., Jordan, C.J., Monteys, X., Pellicer, X.M. & Sheehy, M. (2018) BRITICE glacial map, version 2: a map and GIS database of glacial landforms of the last British-Irish Ice Sheet. *Boreas*, 47(1), 11–e8.

Clubb, F.J., Mudd, S.M., Milodowski, D.T., Valters, D.A., Slater, L.J., Hurst, M.D. & Limaye, A.B. (2017) Geomorphometric delineation of floodplains and terraces from objectively defined topographic thresholds. *Earth Surface Dynamics*, 5(3), 369–385.

Corbett, L.B., Bierman, P.R., Brown, T.A., Caffee, M.W., Fink, D., Freeman, S. P. H.T., Hidy, A.J., Rood, D.H., Wilcken, K.M. & Woodruff, T.E. (2022) Clean quartz matters for cosmogenic nuclide analyses: an exploration of the importance of sample purity using the Cronus-N reference material. *Quaternary Geochronology*, 73, 101403. Available from: https://www.sciencedirect.com/science/article/pii/S1871101422001510

Coulthard, T.J., Neal, J.C., Bates, P.D., Ramirez, J., de Almeida, G. A.M. & Hancock, G.R. (2013) Integrating the LISFLOOD-FP 2D hydrodynamic model with the CAESAR model: implications for modelling landscape evolution. *Earth Surface Processes and Landforms*, 38(15), 1897–1906.

Cyr, A.J., Granger, D.E., Olivetti, V. & Molin, P. (2010) Quantifying rock uplift rates using channel steepness and cosmogenic nuclide-determined erosion rates: examples from northern and southern Italy. *Lithosphere*, 2(3), 188–198.

Delunel, R., Schlunegger, F., Valla, P.G., Dixon, J., Glotzbach, C., Hippe, K., Kober, F., Molliex, S., Norton, K.P., Salcher, B., Wittmann, H., Akçar, N. & Christl, M. (2020) Late-Pleistocene catchment-wide denudation patterns across the European Alps. *Earth-Science Reviews* 211.

Delunel, R., van der Beek, P.A., Carcaillet, J., Bourlès, D.L. & Valla, P.G. (2010) Frost-cracking control on catchment denudation rates: insights from in situ produced 10Be concentrations in stream sediments (Ecrins-Pelvoux massif, French Western Alps). *Earth and Planetary Science Letters*, 293(1-2), 72–83. Available from: https://doi.org/10.1016/j.epsl.2010.02.020

DiBiase, R.A. (2018) Short communication: increasing vertical attenuation length of cosmogenic nuclide production on steep slopes negates topographic shielding corrections for catchment erosion rates. *Earth Surface Dynamics*, 6(4), 923–931.

Dunai, T.J. (2010) *Cosmogenic nuclides: principles, concepts and applications in the earth surface sciences*. Cambridge University Press.

Egholm, D.L., Knudsen, M.F. & Sandiford, M. (2013) Lifespan of mountain ranges scaled by feedbacks between landsliding and erosion by rivers. *Nature*, 498(7455), 475–478.

Fülöp, R.H., Wacker, L. & Dunai, T.J. (2015) Progress report on a novel in situ 14C extraction scheme at the University of Cologne. *Nuclear Instruments and Methods in Physics Research, Section B: Beam Interactions with Materials and Atoms*, 361, 20–24.

Fame, M.L., Owen, L.A., Spotila, J.A., Dortch, J.M. & Caffee, M.W. (2018) Tracking paraglacial sediment with cosmogenic 10Be using an example from the northwest Scottish Highlands. *Quaternary Science Reviews*, 182, 20–36. Available from: https://doi.org/10.1016/j.quascirev.2017.12.017

Fieman, D.M., Attal, M. & Addy, S. (2020) Geomorphic response of a mountain gravel-bed river to an extreme flood in Aberdeenshire, Scotland. *Scottish Journal of Geology*, 56, 2019–005.

Firth, C.R. & Stewart, I.S. (2000) Postglacial tectonics of the Scottish glacio-isostatic uplift centre. *Quaternary Science Reviews*, 19(14-15), 1469–1493.

Flint, J.J. (1974) Stream gradient as a function of order, magnitude, and discharge. *Water Resources Research*, 10(5), 969–973.

Godard, V., Bourlès, D.L., Spinabella, F., Burbank, D.W., Bookhagen, B., Fisher, G.B., Moulin, A. & Léanni, L. (2014) Dominance of tectonics over climate in himalayan denudation. *Geology*, 42(3), 243–246.

Google Maps (2023) Google maps. Available at: Google Earth pro [accessed July 2023].

Gosse, J.C. & Phillips, F.M. (2001) Terrestrial in situ cosmogenic nuclides: theory and application. *Quaternary Science Reviews*, 20(14), 1475–1560. Available from: https://www.sciencedirect.com/science/article/pii/S0277379100001712

Granger, D.E., Kirchner, J.W. & Finkel, R. (1996) Spatially averaged long-term erosion rates measured from in situ-produced cosmogenic nuclides in alluvial sediment. *Journal of Geology*, 104(3), 249–257.

Granger, D.E. & Smith, A.L. (2000) Dating buried sediments using radioactive decay and muogenic production of 26Al and 10Be. *Nuclear Instruments and Methods in Physics Research, Section B: Beam Interactions with Materials and Atoms*, 172(1-4), 822–826.

Gulbransen, E.A., Andrew, K.F. & Brassart, F.A. (1963) The oxidation of graphite at temperatures of 600°c to 1500°c and at pressures of 2 to 76 torr of oxygen. *Journal of The Electrochemical Society*, 110(6), 476. Available from: https://doi.org/10.1149/1.2425797

Hack, J.T., Seaton, F.A. & Nolan, T.B. (1957) Studies of longitudinal stream profiles in Virginia and Maryland United States Department of the Interior. Report, Available from: https://pubs.usgs.gov/pp/0294b/report.pdf

Harel, M.A., Mudd, S.M. & Attal, M. (2016) Global analysis of the stream power law parameters based on worldwide 10Be denudation rates. *Geomorphology*, 268, 184–196. Available from: https://doi.org/10.1016/j.geomorph.2016.05.035

Hippe, K. (2017) Constraining processes of landscape change with combined in situ cosmogenic 14C-10Be analysis. *Quaternary Science Reviews*, 173, 1–19. Available from: https://doi.org/10.1016/j.quascirev.2017.07.020

Hippe, K., Jansen, J.D., Skov, D.S., Lupker, M., Ivy-Ochs, S., Kober, F., Zeilinger, G., Capriles, J.M., Christl, M., Maden, C., Vockenhuber, C. & Egholm, D.L. (2021) Cosmogenic in situ 14C-10Be reveals abrupt Late Holocene soil loss in the Andean Altiplano. *Nature Communications* 12(1). Available from: https://doi.org/10.1038/s41467-021-22825-6

Hippe, K., Kober, F., Wacker, L., Fahrni, S.M., Ivy-Ochs, S., Akar, N., Schlüchter, C. & Wieler, R. (2013) An update on in situ cosmogenic 14C analysis at ETH zürich. *Nuclear Instruments and Methods in Physics Research Section B: Beam Interactions with Materials and Atoms*, 294, 81–86. Proceedings of the Twelfth International Conference on Accelerator Mass Spectrometry, Wellington, New Zealand, 20-25 March 2011.

Horii, N., Kuzuu, N.Y. & Horikoshi, H. (2021) Promoting vitreous silica devitrification by placement on a NaCl grain at 800 °C-1150 °c. *Japanese Journal of Applied Physics* 60. Available from: https://api.semanticscholar.org/CorpusID:233954680

International Atomic Energy Agency (2024) IAEA - Nuclear Data Section. Available from: https://www-nds.iaea.org/ [Accessed Feb 2024].

Jansen, J.D., Fabel, D., Bishop, P., Xu, S., Schnabel, C. & Codilean, A.T. (2011) Does decreasing paraglacial sediment supply slow knickpoint retreat?. *Geology*, 39(6), 543–546.

Jull, A. J.T., Scott, E.M. & Bierman, P.R. (2015) The Cronus-Earth inter-comparison for cosmogenic isotope analysis. *Quaternary Geochronology*, 26, 3–10. Available from: https://api.semanticscholar.org/CorpusID:128750255

Kim, J.Y. (2004) *Controls over bedrock channel incision [PhD thesis]*. University of Glasgow.

Kirby, E. & Whipple, K.X. (2012) Expression of active tectonics in erosional landscapes. *Journal of Structural Geology*, 44, 54–75. Available from: https://doi.org/10.1016/j.jsg.2012.07.009

Kober, F., Hippe, K., Salcher, B., Grischott, R., Zurfluh, R., Hajdas, I., Wacker, L., Christl, M. & Ivy-Ochs, S. (2019) Postglacial to Holocene landscape evolution and process rates in steep alpine catchments. *Earth Surface Processes and Landforms*, 44(1), 242–258.

Kohl, C.P. & Nishiizumi, K. (1992) Chemical isolation of quartz for measurement of in-situ-produced cosmogenic nuclides. *Geochimica et Cosmochimica Acta*, 56, 3583–3587. Available from: https://api.semanticscholar.org/CorpusID:95525773

Lal, D. (1991) Cosmic ray labeling of erosion surfaces: in situ nuclide production rates and erosion models: earth and planetary science letters. *Earth and Planetary Science Letters*, 104(2-4), 424–439.

Laptev, A.M. & Bram, M. (2024) Sublimation rate of solid NaCl powders and evaporation rate of liquid NaCl upon heating in vacuum and air. Available from: https://api.semanticscholar.org/CorpusID:273183769

Lifton, N.A., Jull, A. J.T. & Quade, J. (2001) A new extraction technique and production rate estimate for in situ cosmogenic 14C in quartz. *Geochimica et Cosmochimica Acta*, 65, 1953–1969. Available from: https://api.semanticscholar.org/CorpusID:128409054

Lifton, N., Sato, T. & Dunai, T.J. (2014) Scaling in situ cosmogenic nuclide production rates using analytical approximations to atmospheric cosmic-ray fluxes. *Earth and Planetary Science Letters*, 386, 149–160. Available from: https://www.sciencedirect.com/science/article/pii/S0012821X13006316

Lifton, N., Sato, T. & Dunai, T.J. (2014) Scaling in situ cosmogenic nuclide production rates using analytical approximations to atmospheric cosmic-ray fluxes. *Earth and Planetary Science Letters*, 386, 149–160.

Lifton, N., Wilson, J. & Koester, A. (2023) Technical note: studying lithium metaborate fluxes and extraction protocols with a new, fully automated in situ cosmogenic ^{14}C processing system at PRIME Lab. *Geochronology* 5(2): 361–375. Available from: https://gchron.copernicus.org/articles/5/361/2023/

Linton, D.L. (1949) Some scottish river captures re-examined. *Scottish Geographical Magazine*, 65(3), 123–132.

Lupker, M., Hippe, K., Wacker, L., Kober, F., Maden, C., Braucher, R., Bourlès, D., Romani, J. R.V. & Wieler, R. (2015) Depth-dependence of the production rate of in situ 14C in quartz from the Leymon high core, Spain. *Quaternary Geochronology*, 28, 80–87.

Lupker, M., Hippe, K., Wacker, L., Steinemann, O., Tikhomirov, D., Maden, C., Haghipour, N. & Synal, H.-A. (2019) In-situ cosmogenic 14C analysis at ETH Zürich: characterization and performance of a new extraction system. *Nuclear Instruments and Methods in Physics Research Section B: Beam Interactions with Materials and Atoms*, 457, 30–36. Available from: https://www.sciencedirect.com/science/article/pii/S0168583X19305178

Lupker, M., Lavé, J., France-Lanord, C., Christl, M., Bourlès, D., Carcaillet, J., Maden, C., Wieler, R., Rahman, M., Bezbaruah, D. & Xiaohan, L. (2017) 10Be systematics in the Tsangpo-Brahmaputra catchment: the cosmogenic nuclide legacy of the eastern Himalayan syntaxis. *Earth Surface Dynamics*, 5(3), 429–449.

Mehrer, H. (2007) Dependence of diffusion on temperature and pressure. In *Diffusion in solids: fundamentals, methods, materials, diffusion-controlled processes*, Springer Berlin Heidelberg: Berlin, Heidelberg; 127–149. Available from: https://doi.org/10.1007/978-3-540-71488-0_8

Mergelov, N.S., Mueller, C.W., Prater, I., Shorkunov, I.G., Dolgikh, A.V., Zazovskaya, E.P., Shishkov, V., Krupskaya, V., Abrosimov, K.N., Cherkinsky, A. & Goryachkin, S.V. (2018) Alteration of rocks by endolithic organisms is one of the pathways for the beginning of soils on earth. *Scientific Reports* 8. Available from: https://api.semanticscholar.org/CorpusID:3432728

Mudd, S.M. (2017) Detection of transience in eroding landscapes. *Earth Surface Processes and Landforms*, 42(1), 24–41.

Mudd, S.M., Attal, M., Milodowski, D.T., Grieve, S. W.D. & Valters, D.A. (2014) A statistical framework to quantify spatial variation in channel gradients using the integral method of channel profile analysis. *Journal of Geophysical Research: Earth Surface*, 119(2), 138–152.

Mudd, S.M., Clubb, F.J., Grieve, S. W.D., Milodowski, D.T., Gailleton, B., Hurst, M.D., Valters, D.V., Wickert, A.D. & Hutton, E. W.H. (2023) LSDtopotools/LSDTopoTools2: LSDTopoTools2 v0.8. Available from: https://zenodo.org/record/7892465

Mudd, S.M., Harel, M.A., Hurst, M.D., Grieve, S. W.D. & Marrero, S.M. (2016) The CAIRN method: automated, reproducible calculation of catchment-averaged denudation rates from cosmogenic nuclide concentrations. *Earth Surface Dynamics*, 4(3), 655–674.

Nichols, K.A. & Goehring, B.M. (2019) Isolation of quartz for cosmogenic in situ chem ^{14}C analysis. *Geochronology* 1(1): 43–52. Available from: https://gchron.copernicus.org/articles/1/43/2019/

Ordnance Survey (2021) OS terrain 5. Available from: https://digimap.edina.ac.uk

Parker, G. (1991) Possible to formulate quantitative theories of downstream fining that rely solely on the mechanism of selective sorting, e. g., Diegaard (1980) and Di Silvio (1984). In the case of gravel streams the situation is much less clear. The abrasion rate. *Journal of Hydraulic Engineering*, 117(2), 131–147.

Raven, E.K., Lane, S.N., Ferguson, R.I. & Bracken, L.J. (2009) The spatial and temporal patterns of aggradation in a temperate, upland, gravel-bed river. *Earth Surface Processes and Landforms*, 34(9), 1181–1197. Available from: https://doi.org/10.1002/esp.1783

Reimer, P.J., Austin, W. E.N., Bard, E., Bayliss, A., Blackwell, P.G., Ramsey, C.B., Butzin, M., Cheng, H., Edwards, R.L. & Friedrich, M. (2020) The IntCal20 Northern Hemisphere radiocarbon age calibration curve (0–55 cal kBP). *Radiocarbon*, 62(4), 725–757.

Robertson Rintoul, M. S.E. (1986) A quantitative soil stratigraphic approach to the correlation and dating of post glacial river terraces in Glen Feshie, western Cairngorms. *Earth Surface Processes and Landforms*, 11(6), 605–617.

Rumsby, B.T., Brasington, J., Langham, J.A., McLelland, S.J., Middleton, R. & Rollinson, G. (2008) Monitoring and modelling particle and reach-scale morphological change in gravel-bed rivers: applications and challenges. *Geomorphology*, 93(1-2), 40–54.

Safran, E.B., Bierman, P.R., Aalto, R., Dunne, T., Whipple, K.X. & Caffee, M. (2005) Erosion rates driven by channel network incision in the Bolivian Andes. *Earth Surface Processes and Landforms*, 30(8), 1007–1024.

Schaller, M., Ehlers, T.A., Blum, J.D. & Kallenberg, M.A. (2009) Quantifying glacial moraine age, denudation, and soil mixing with cosmogenic nuclide depth profiles. *Journal of Geophysical Research: Earth Surface*, 114(1), 1–18.

Scherler, D., Bookhagen, B. & Strecker, M.R. (2014) Tectonic control on 10Be-derived erosion rates in the Garhwal Himalaya, India. *Journal of Geophysical Research: Earth Surface*, 119(2), 83–105.

Schiffer, M., Stolz, A., López, D.A., Spanier, R., Herb, S., Müller-Gatermann, C., Heinze, S., Binnie, S., Melchert, J., Kivel, N., Schumann, D., Rethemeyer, J., Dunai, T. & Dewald, A. (2020) Method developments for accelerator mass spectrometry at CologneAMS, 53Mn/3He burial dating and ultra-small 14CO2 samples. *Global and Planetary Change* 184(May 2019): 103053. Available from: https://doi.org/10.1016/j.gloplacha.2019.103053

Scott, E.M., Naysmith, P. & Cook, G.T. (2018) Why do we need 14C inter-comparisons?: the Glasgow -14C inter-comparison series, a reflection over 30 years. *Quaternary Geochronology*, 43, 72–82. Available from: https://www.sciencedirect.com/science/article/pii/S1871101417300730

Shennan, I., Milne, G. & Bradley, S. (2009) Late Holocene relative land- and sea-level changes: providing information for stakeholders. *GSA Today*, 19(9), 52–53.

Sissons, J.B. (1974) Late-glacial marine erosion in Scotland. *Boreas*, 3(2), 41–48.

Slater, L.J., Singer, M.B. & Kirchner, J.W. (2015) Hydrologic versus geomorphic drivers of trends in flood hazard. *Geophysical Research Letters*, 42(2), 370–376.

Slosson, J.R., Hoke, G.D. & Lifton, N. (2022) Non-Steady-State 14C-10Be and Transient Hillslope Dynamics in Steep High Mountain Catchments. *Geophysical Research Letters*, 49(24), 1–10.

Stbner, K., Balco, G. & Schmeisser, N. (2023) Riversand: a new tool for efficient computation of catchmentwide erosion ratES. *Radiocarbon*, 2023, 1–14.

Stone, J.O. (2000) Isotope production T , T ,. *Journal of Geophysical Research*, 105(1), 753–759.

Stover, S.C. & Montgomery, D.R. (2001) Channel change and flooding, Skokomish River, Washington. *Journal of Hydrology*, 243(3-4), 272–286.

Sulaymonova, V.A., Fuchs, M.C., Gloaguen, R., Möckel, R., Merchel, S., Rudolph, M. & Krbetschek, M.R. (2018) Feldspar flotation as a quartz-purification method in cosmogenic nuclide dating: A case study of fluvial sediments from the pamir. *MethodsX*, 5, 717–726. Available from: https://api.semanticscholar.org/CorpusID:51941406

Vermeesch, P. (2007) CosmoCalc: An Excel add-in for cosmogenic nuclide calculations. *Geochemistry, Geophysics, Geosystems*, 8(8), 1–14.

von Blanckenburg, F. (2005) The control mechanisms of erosion and weathering at basin scale from cosmogenic nuclides in river sediment. *Earth and Planetary Science Letters*, 237(3-4), 462–479.

Wacker, L., Fahrni, S.M., Hajdas, I., Molnár, M., Synal, H.A., Szidat, S. & Zhang, Y. (2013) A versatile gas interface for routine radiocarbon analysis with a gas ion source. *Nuclear Instruments & Methods in Physics Research Section B-beam Interactions With Materials and Atoms*, 294, 315–319. Available from: https://api.semanticscholar.org/CorpusID:96623386

Whitbread, K., Jansen, J., Bishop, P. & Attal, M. (2015) Substrate, sediment, and slope controls on bedrock channel geometry in postglacial streams. *Journal of Geophysical Research: Earth Surface*, 120, 779–798. Available from: https://doi.org/10.1130/B35334.1

Wierzchos, J., Davila, A.F., Artieda, O., Cámara-Gallego, B., de los Ríos, A., Nealson, K.H., Valea, S., García-González, M.T. & Ascaso, C. (2013) Ignimbrite as a substrate for endolithic life in the hyper-arid atacama desert: implications for the search for life on mars. *Icarus*, 224, 334–346. Available from: https://api.semanticscholar.org/CorpusID:122327828

Williams, R.D., Lamy, M.L., Maniatis, G. & Stott, E. (2020) Three-dimensional reconstruction of fluvial surface sedimentology and topography using personal mobile laser scanning. *Earth Surface Processes and Landforms*, 45(1), 251–261.

Williams, R.D., Measures, R., Hicks, D.M. & Brasington, J. (2016) Assessment of a numerical model to reproduce event-scale erosion and deposition distributions in a braided river. *Water Resources Research*, 52(8), 6621–6642. Available from: https://doi.org/10.1002/2015WR018491

Wittmann, H. & von Blanckenburg, F. (2009) Cosmogenic nuclide budgeting of floodplain sediment transfer. *Geomorphology*, 109(3-4), 246–256. Available from: https://doi.org/10.1016/j.geomorph.2009.03.006

Wittmann, H., von Blanckenburg, F., Kruesmann, T., Norton, K.P. & Kubik, P.W. (2007) Relation between rock uplift and denudation from cosmogenic nuclides in river sediment in the Central Alps of

Switzerland. *Journal of Geophysical Research: Earth Surface*, 112(4), 1–20.

Wittmann, H., von Blanckenburg, F., Maurice, L., Guyot, J.L., Filizola, N. & Kubik, P.W. (2011) Sediment production and delivery in the Amazon River basin quantified by in situ-produced cosmogenic nuclides and recent river loads. *Bulletin of the Geological Society of America*, 123(5), 934–950.

Wobus, C.W., Crosby, B.T. & Whipple, K.X. (2006) Hanging valleys in fluvial systems: Controls on occurrence and implications for landscape evolution. *Journal of Geophysical Research: Earth Surface*, 111(2), 1–14.

Young, J. A.T. (1975) Ice wastage in glen Feshie, Inverness-shire. *Scottish Geographical Magazine*, 91(2), 91–101.

Young, J. A.T. (1976) The Terraces of Glen Feshie, Inverness-shire. *Earth and Environmental Science Transactions of The Royal Society of Edinburgh* 69(22).

SUPPORTING INFORMATION

Additional supporting information can be found online in the Supporting Information section at the end of this article.

How to cite this article: Towers, A.H., Mudd, S.M., Attal, M., Clubb, F.J., Binnie, S.A., Dunai, T.J. et al. (2025) Denudation rates and Holocene sediment storage dynamics inferred from *in situ* ^{14}C concentrations in the Feshie basin, Scotland. *Earth Surface Processes and Landforms*, 50(4), e70043. Available from: https://doi.org/10.1002/esp.70043